Comparative and population genomics landscape of *Phellinus noxius*: a hypervariable fungus causing root rot in trees

Chia-Lin Chung¶[1,2], Tracy J. Lee[3,4,5], Mitsuteru Akiba[6], Hsin-Han Lee[1], Tzu-Hao Kuo[3], Dang Liu[3,7], Huei-Mien Ke[3], Toshiro Yokoi[6], Marylette B Roa[3,8], Meiyeh J Lu[3], Ya-Yun Chang[1], Pao-Jen Ann[9], Jyh-Nong Tsai[9], Chien-Yu Chen[10], Shean-Shong Tzean[1], Yuko Ota[6,11], Tsutomu Hattori[6], Norio Sahashi[6], Ruey-Fen Liou[1,2], Taisei Kikuchi[12] and Isheng J Tsai¶[3,4,5,7]

[1]Department of Plant Pathology and Microbiology, National Taiwan University, Taiwan

[2]Master Program for Plant Medicine, National Taiwan University, Taiwan

[3]Biodiversity Research Center, Academia Sinica, Taipei, Taiwan

[4]Biodiversity Program, Taiwan International Graduate Program, Academia Sinica and National Taiwan Normal University

[5]Department of Life Science, National Taiwan Normal University

[6]Department of Forest Microbiology, Forestry and Forest Products Research Institute, Tsukuba, Japan

[7]Genome and Systems Biology Degree Program, National Taiwan University and Academia Sinica, Taipei, Taiwan

[8]Philippine Genome Center, University of the Philippines, Diliman, Quezon City, Philippines 1101

[9]Plant Pathology Division, Taiwan Agricultural Research Institute

[10]Department of Bio-industrial Mechatronics Engineering, National Taiwan University, Taiwan

[11]College of Bioresource Sciences, Nihon University, Fujisawa, Japan

[12]Division of Parasitology, Faculty of Medicine, University of Miyazaki, Miyazaki, Japan

¶ These authors contributed equally to this work

Correspondence: Chia-Lin Chung, clchung@ntu.edu.tw, Taisei Kikuchi (taisei_kikuchi@med.miyazaki-u.ac.jp) and Isheng Jason Tsai (ijtsai@gate.sinica.edu.tw)

Abstract

The order Hymenochaetales of white rot fungi contain some of the most aggressive wood decayers causing tree deaths around the world. Despite their ecological importance and the impact of diseases they cause, little is known about the evolution and transmission patterns of these pathogens. Here, we sequenced and undertook comparative genomics analyses of Hymenochaetales genomes using brown root rot fungus *Phellinus noxius*, wood-decomposing fungus *Phellinus lamaensis*, laminated root rot fungus *Phellinus sulphurascens*, and trunk pathogen *Porodaedalea pini*. Many gene families of lignin-degrading enzymes were identified from these fungi, reflecting their ability as white rot fungi. Comparing against distant fungi highlighted the expansion of 1,3-beta-glucan synthases in *P. noxius*, which may account for its fast-growing attribute. We identified 13 linkage groups conserved within Agaricomycetes, suggesting the evolution of stable karyotypes. We determined that *P. noxius* has a bipolar heterothallic mating system, with unusual highly expanded ~60 kb *A* locus as a result of accumulating gene transposition. We investigated the population genomics of 60 *P. noxius* isolates across multiple islands of the Asia Pacific region. Whole-genome sequencing showed this multinucleate species contains abundant poly-allelic single-nucleotide-polymorphisms (SNPs) with atypical allele frequencies. Different patterns of intra-isolate polymorphism reflect mono-/heterokaryotic states which are both prevalent in nature. We have shown two genetically separated lineages with one spanning across many islands despite the geographical barriers. Both populations possess extraordinary genetic diversity and

54 show contrasting evolutionary scenarios. These results provide a framework to further
55 investigate the genetic basis underlying the fitness and virulence of white rot fungi.
56
57
58

59 ## Introduction

60

61 Under most circumstances, fungi coexist with trees or act as saprotrophs responsible
62 for carbon and nitrogen cycling in forest systems. However, some fungi are also one
63 of the dominant groups of pathogens causing diseases in trees. There has been an
64 emergence of tree disease outbreaks in different parts of the world such as ash
65 dieback (Gross, Holdenrieder, Pautasso, Queloz, & Sieber, 2014), Dutch elm disease
66 (Potter, Harwood, Knight, & Tomlinson, 2011), laminated root rot caused by
67 *Phellinus sulphurascens* (Williams et al., 2014), and brown root rot caused by
68 *Phellinus noxius* (Akiba et al., 2015; P. Ann, Chang, & Ko, 2002; Chung et al., 2015).
69 Factors contributing to this phenomenon include climate change (Goberville et al.,
70 2016) and human activity (Fisher et al., 2012). If interventions are not implemented
71 early and effective, pathogen infections can kill millions of trees and the spread can
72 become very difficult to stop (Cunniffe, Cobb, Meentemeyer, Rizzo, & Gilligan,
73 2016).
74

Hymenochaetales is dominated by wood decay fungi and belongs to Agaricomycetes of Basidiomycota. Most species within this order are saprotrophic but some also exhibit pathogenic lifestyles that have been recorded in major forest incidents as early as 1971 in different parts of the world (Hepting, 1971; Norio Sahashi, Akiba, Ishihara, Ota, & Kanzaki, 2012). In particular, *P. noxius* has a very wide host range, spanning more than 200 broadleaved and coniferous tree species (at least 59 families) including many agricultural, ornamental, and forest trees such as longan, litchi, camphor, banyan, and pine (P. Ann et al., 2002; Norio Sahashi et al., 2014). Inoculation assays showed that only seven out of 101 tested tree cultivars (92 species) exhibited high resistance (P. J. Ann, Lee, & Huang 1999). Despite the recognized importance of *P. noxius* as an emerging pathogen, its genome, evolution and global population genetics is poorly understood. Previous reports based on simple sequence repeat (SSR) markers suggest the existence of highly diversified *P. noxius* populations (Akiba et al., 2015; Chung et al., 2015), but the isolates exhibited little to no host specificity (P. J. Ann et al., 1999; Nandris, Nicole, & Geiger, 1987; N. Sahashi, Akiba, Ishihara, Miyazaki, & Kanzaki, 2010). Currently, no gold standard genomes (Chain et al., 2009) are available for this group of wood decay fungi, which is a necessary step toward a better knowledge of their diversity, ecology and evolution.

The life cycle of *P. noxius* (P. Ann et al., 2002) is thought to be similar to other important root-rotting basidiomycetes, such as *Armillaria mellea* and *Heterobasidion annosum*. The new infection can start from previously infected plants/stumps or colonized wood debris, from which the mycelium of *P. noxius* grows to infect the

98 lateral and tap roots of the host tree (P. Ann et al., 2002). An invasion to the cortex
99 and lignified xylem is usually observed (T.-T. Chang, 1992), sometimes accompanied
100 by gradual expansion of the mycelial mat to the basal stem (Fig. 1A). Diseased trees
101 with decayed roots may then show symptoms of foliar chlorosis, thinning leaves,
102 defoliation, and eventually decline within a few months to several years. The
103 damaged and fragile roots (Fig. 1B) also make the trees easily toppled over by strong
104 winds and heavy rains. Basidiocarps are occasionally formed on trunks of infected
105 trees (Fig. 1C-D). The sexual reproduction system of *P. noxius* has remained
106 unclarified, partly due to the lack of clamp connections for diagnosing compatibility
107 (P. Ann et al., 2002).
108
109 Brown root rot disease caused by *P. noxius* is widespread in tropical and subtropical
110 areas in Southeast and East Asia, Oceania, Africa, Central America and the Caribbean.
111 The geographical distribution appears to be related to the growth temperature range of
112 *P. noxius*: 10-12^{o}C to 36 ^{o}C, with optimum growth at 30 ^{o}C. In the past 20 years,
113 brown root rot disease has become a serious threat to a variety of perennial fruit trees,
114 ornamental and landscape trees, and shade trees in Taiwan (Chung et al., 2015) and in
115 Ryukyu and Ogasawara Islands of Japan (Akiba et al., 2015). In Australia, it occurs in
116 the natural and commercial plantation forests and orchards along the east coast, and
117 has killed many trees in the Greater Metropolitan area of Brisbane Queensland
118 (Schwarze, Jauss, Spencer, Hallam, & Schubert, 2012). In West Africa and China,
119 brown root rot was reported as the most devastating root disease attacking the rubber
120 plantations (Nandris et al., 1987). Trees in urban areas and plantation forests in Hong

121 Kong and Macao have also been seriously affected (Huang, Sun, Bi, Zhong, & Hu,
122 2016; Wu et al., 2011). Field observations support the root-to-root spread as a major
123 transmission mode of the epidemic. Recent population genetics studies based on SSR
124 markers revealed highly diverse genotypes within populations and nearly identical
125 genotypes from neighboring infected trees, suggesting that *P. noxius* spreads over
126 short distances via root-to-root contact of the hosts, and the genetically variable
127 basidiospores are likely involved in long-distance dispersal and the establishment of
128 unique clones in new disease foci (Akiba et al., 2015; Chung et al., 2015).
129
130 In the present study, we aimed to further understand the evolution, reproductive
131 system, and epidemiology in *P. noxius*, on the whole genomic basis. To achieve this,
132 we first sequenced, assembled and annotated the genome sequences of four species
133 from Hymenochaetales: *Phellinus noxius*, *Phellinus lamaensis* (wood decomposing
134 fungus that causes a white pocket rot only on dead heartwood trees), *Phellinus*
135 *sulphurascens* (syn. *Coniferiporia sulphurascens* (Zhou, Vlasák, & Dai, 2016);
136 pathogen responsible for laminated root rot in Douglas-fir/ true fir), and
137 *Porodaedalea pini* (syn. *Phellinus pini;* trunk pathogen of conifers). Focusing on *P.*
138 *noxius*, its ~31Mb genome was sequenced to a high level of completion containing
139 telomere-to-telomere chromosome sequences. By comparing against representative
140 species of Basidiomycota, we investigated the genomic conservations and
141 specialisations of this group and how these features possibly relate to the lifestyle of a
142 wood-decayer. Second, we collected *P. noxius* isolates from diseased trees across
143 Taiwan and Japanese offshore islands in 2007-2014. We sequenced the

whole-genomes of these 60 isolates and realigned against the *P. noxius* reference genome to identify single nucleotide polymorphisms (SNPs). Based on the genetic variation, the phylogenetic relationship of *P. noxius* populations within this Asia Pacific region was determined. We also quantified the extent of intra-isolate polymorphism to infer the frequencies of morphologically indistinguishable mono- and heterokaryons at infection sites. This allowed the confirmation of heterokaryosis is not necessary for pathogenicity in *P. noxius*.

Methods

Strain preparation and sequencing

Genome sequencing of three *Phellinus* species and *P. pini* (Text S1) was performed using both Pacific Biosciences (*P. noxius*, *P. lamaensis*, *P. sulphurascens* and *P. pini*) and Illumina (*P. noxius*) platforms. DNA was isolated using the CTAB method (Chung et al., 2015). At least 15 μg DNA was used for a 20 kb library prep according to the manufacturer's instructions. Sequencing was performed on a Pacific Biosciences RS II system using 8 SMRT cell per run, P6C4 chemistry and 360 min movie time. A total of 5-7 SMRT cells were run per species yielding a raw depth of coverage of 173-266X. For samples underwent *de novo* assembly, genomic DNA were sheared in M220 Focused-ultrasonicator™ (Covaris) in microTUBE-50 (Covaris) under 250bp program (duty factor 20%, treatment for 120 sec) with gel size selection after adaptor ligation. For population resequencing samples, genomic DNA were

sheared in microTUBE-130 (Covaris) using 500bp shearing program (duty factor 10%, treatment for 60 sec). Genomic libraries were prepared using TruSeq DNA LT Sample Prep Kit (Illumina). Input of 1 μg sheared DNA was used for end-repair, A-tailing, adaptor ligation, and gel size selection. Size range at 600-700bps range was selected from gel and amplified by 5 cycles of PCR. In addition, Illumina mate-pair libraries were generated using 8 μg of genomic DNA with gel size selection of tagmented DNA at 2-4 kb, 4-7 kb, 7-10 kb, and 10-20 kb, and amplified by 10~15 cycles of PCR. These libraries were normalized by KAPA Library Quantification Kit (KAPA Biosystems), and pooled equally for PE2*300 sequencing on MiSeq V2 sequencer. The descriptions of the raw genomic data are available on Table S1.

To aid annotation for each of the species in this study, 7- to 21-day old mycelia from PDA cultures were used for RNA-seq. RNA-seq libraries were constructed using the Illumina TruSeq Stranded mRNA HT Sample Prep Kit with the dual index barcoded adaptors. Input of 3 μg of total RNA was used for each sample for two rounds of oligo-dT bead enrichment, and the ligated cDNA were amplified by 10 cycles of PCR. The Stranded mRNA libraries were quantified by Qubit and molar concentrations normalized against the KAPA Library Quantification Kit (KAPA Biosystems) for Illumina platform. The transcriptome libraries were pooled at equal molar concentrations, and PE2*151nt multiplexed sequencing was conducted on HiSeq 2500 sequencer. The descriptions of the raw RNA-seq data are available on Table S2.

Nuclear quantification

Nuclei in the growing hyphal tips were stained following the procedure described by Chung et al. (2015). The mycelium on the slide was mounted in 20 μl of a DAPI (4',6-diamidino-2-phenylindole) solution (10 μg/ml in ddH_2O) for an hour, destained in ddH_2O for 30 min, then observed under a OLYMPUS BX41 microscope (Shinjuku-ku, Tokyo, Japan) equipped with filter cube U-MWU2 (BP 330–385 nm, LP 420 nm). Images were captured by using a Canon (Ohta-ku, Tokyo, Japan) digital camera EOS 700D. One hundred hyphal cells per strain were counted.

Genome assembly

Genome assembly of different species was carried out with Falcon (ver 0.5.0; Chin et al., 2016) and were improved using Quiver (Chin et al., 2013) and finisherSC (Lam, LaButti, Khalak, & Tse, 2015). For assembly of individual strains of *P. noxius*, Illumina paired end reads were trimmed with Trimmomatic (ver 0.32; options LEADING:30 TRAILING:30 SLIDINGWINDOW:4:30 MINLEN:50; Bolger, Lohse, & Usadel, 2014) and subsequently assembled using SPAdes (ver 3.7.1; Bankevich et al., 2012). Multiple mate-pair reads were available for three strains of *P. noxius* (KPN91, A42 and 718-S1) and they were assembled using ALLPATH-LG (ver 49688; Butler et al., 2008) assembler and improved using Pilon (Walker et al., 2014). The *P. noxius* assembly was further merged with metassembler (ver 1.5; Wences & Schatz, 2015), misassemblies were identified using REAPR (ver 1.0.18; Hunt et al., 2013) and manually corrected.

Gene predictions and functional annotation

For *P. noxius*, the gene predictor Augustus (ver3.2.1; Stanke, Tzvetkova, & Morgenstern, 2006) was trained on a gene training set of complete core genes from CEGMA (ver2.5; Parra, Bradnam, & Korf, 2007) and subsequently used for manual curation of ~1000 genes. Annotation was then run by providing introns as evidence from RNA-seq data. For *P. lamaensis*, *P. sulphurascens* and *P. pini*, genes were predicted using Braker1 (ver 1.9; Hoff, Lange, Lomsadze, Borodovsky, & Stanke, 2016) pipeline that automatically use RNA-seq mappings as evidence hints and retraining of GeneMark-ES (Borodovsky & Lomsadze, 2011) and Augustus. Gene product description was assigned using blast2go (ver 4.0.7; Conesa et al., 2005) and GO term assignment were provided by ARGOT2.5 (Lavezzo, Falda, Fontana, Bianco, & Toppo, 2016). The web server dbCAN (HMMs 5.0, last accessed September 5 2016; Yin et al., 2012) was used to predict CAZymes from the protein sequences of all species, while AntiSMASH (ver 3.0; Weber et al., 2015) was used to predict secondary metabolite gene clusters. For dbCAN results, only hits with <= 1 x 10e-5 e-value and >= 30% HMM coverage were considered, while overlapping domains were resolved by choosing hits with the smallest *P*-value. Proteome completeness were assessed with BUSCO (ver 2.0; Simão, Waterhouse, Ioannidis, Kriventseva, & Zdobnov, 2015) using the Basidiomycota dataset.

Comparative genomics analysis

Gene families were determined by OrthoFinder (ver 1.0.6; Emms & Kelly, 2015). Then, MAFFT (ver 7.271; Katoh & Standley, 2014) was used to align sequences in each of 1,127 single-copy orthogroups. Alignments results with less than 10%

alignment gaps were concatenated, and the outcome was taken to compute a maximum likelihood phylogeny using RAxML (ver 7.7.8; Stamatakis, 2006) with 100 bootstrap replicates. Gene family gain and loss in different positions along the global phylogeny leading to *P. noxius* were inferred using dollop (Felsenstein, 2005). Pfam and GO enrichments were carried out on these gene families using TopGO (ver 2.10.0; Alexa & Rahnenfuhrer, 2016). Sequences to be included in the phylogenetic tree for NACHT domain containing genes were selected on the basis of the presence of pfam domain PF05729.

MAT locus

Homologs of the conserved genes in mating locus *A* and *B* were annotated in *P. noxius*, *P. pini*, *P. sulphurascens* and *P. lamaensis* (e-value < 10^{-5}) then subjected to InterProScan 5 (ver 5.20-59.0; Jones et al., 2014) and Pfam (ver 30.0; Finn et al., 2016) for protein signature prediction. Syntenic alignment of *A* locus among *Phellinus* spp. and other species (sequences/annotations retrieved from Joint Genome Institute MycoCosm (Grigoriev et al., 2014)) was plotted using genoPlotR package (Guy, Roat Kultima, & Andersson, 2010) in R. The sequences of *A* locus in KPN91, 718-S1 and A42 were further compared by MUMmer (ver 3.20; Stefan Kurtz et al., 2004) and PipMaker (http://pipmaker.bx.psu.edu/cgi-bin/pipmaker?basic; Schwartz et al., 2000). For identification of candidate pheromone genes, all the potential open reading frames were filtered for small peptides with C-terminal CaaX motif, then searched for pheromone homologies against Pfam-A and scanned for farnesylation signal by PrePs (http://mendel.imp.ac.at/PrePS/; Maurer-Stroh & Eisenhaber, 2005).

258

259 The sequences of *HD* and *STE3* genes were analyzed for 10 single-basidiospore
260 isolates originating from a basidiocarp by the dideoxy termination method (primers
261 listed in Table S3). Long-range PCR followed by primer walking was performed to
262 sequence the highly diverse regions containing *HD1-HD2* in *A* locus. The outer
263 primers were designed manually based on the alignment of all the isolates; the inner
264 primers were developed step-by-step according to previous sequencing results. The
265 PCR reaction was performed in 30-μl reaction mixture containing 50 to 100 ng
266 genomic DNA, 0.2 mM dNTP, 1X Ex Taq buffer [proprietary, containing 20mM
267 Mg^{2+}] (Takara Bio Inc., Japan), 0.67 μM forward and reverse primers, and TaKaRa
268 Ex Taq® DNA polymerase (Takara Bio Inc., Japan). The thermal cycling parameters
269 were 1 cycle of 95°C for 3 min, 30 cycles of 95°C for 30 s, 54°C for 30 s, and 72°C
270 for 60–270 s (according to different product sizes, ~2 kb/min), and a final extension
271 step of 72°C for 10 min. The PCR products were sequenced by Genomics
272 Biotechnology Inc. (Taipei, Taiwan). DNA trace data were visualized using 4Peaks
273 (http://nucleobytes.com/4peaks) and assembled using DNA Sequence Assembler in
274 DNA Baser (http://www. dnabaser.com).

275

276 *Population genomics*

277 Paired end reads of 60 *P. noxius* strains (description listed in Table S4) were aligned
278 to the KPN91 reference using Smalt (ver 5.7;
279 www.sanger.ac.uk/resources/software/smalt/). Removal of PCR duplicates and bam
280 file sorting were implemented with Picard (http://broadinstitute.github.io/picard/) and

281 samtools (ver 1.3-20-gd49c73b; Li et al., 2009). The first round of variant
282 identification was implemented in Varscan (ver 2.4.0; Koboldt et al., 2012) and
283 degree of heterokaryon was inferred in each strain based on allele frequency and total
284 number of heterozygous SNPs called. The final list of SNPs was ascertained by
285 combining evidences from samtools (ver 1.3-20-gd49c73b; Li et al., 2009) and
286 FreeBayes (ver 1.0.2-16-gd466dde; Garrison & Marth, 2012). A maximum likelihood
287 phylogeny of the SNPs segregating in these 60 strains was produced using FastTree
288 (Price, Dehal, & Arkin, 2009). Plink (ver 1.9; C. C. Chang et al., 2015) was used to
289 subset biallelic SNPs without linkage (filtering options: --maf 0.05 --indep-pairwise
290 50 5 0.2), which were clustered using fastSTRUCTURE (ver 1.0; Raj, Stephens, &
291 Pritchard, 2014) to determine the optimal number of populations. Strains were phased
292 using samtools (ver 1.3-20-gd49c73b; Li et al., 2009) and one haplotype was chosen
293 at random. Consensus sequences were generated from each strain using bcftools (ver
294 1.3.1; Danecek et al., 2011) and population genetics analyses were conducted using
295 Variscan (ver 2.0.3; Vilella, Blanco-Garcia, Hutter, & Rozas, 2005).
296
297

298 ## Results

299

300 *Genomes and annotations of four Hymenochaetales members*

301 We produced a 31.6 Mb *Phellinus noxius* genome reference assembly from a
302 Japanese KPN91 isolate combining both Pacific biosciences and Illumina sequencing

303 platforms (Methods). The nuclear genome of *P. noxius* is assembled into 12 scaffolds
304 with six assembled into chromosomes from telomere to telomere, while the
305 mitochondrial genome is assembled into a single sequence of 163.4 kb. For a
306 comprehensive understanding of genome evolution amongst members of the
307 hymenochaetoid clade, we also sequenced and assembled three additional species: *P.*
308 *sulphurascens, P. lamaensis* and *P. pini*, as well as two more isolates (A42 and
309 718-S1) of *P. noxius*. The three assemblies of *P. noxius* have N50s of 2.4-2.7 Mb,
310 whilst the other three genome assemblies comprise 30.7-53.3 Mb with N50's of 570
311 kb-2.7 Mb.
312
313 A total of 9,833-18,103 genes were predicted in each species, which are 82-94%
314 complete (Table S5). To compare these predicted proteins to those of other
315 basidiomycetes to explore chromosome and gene family evolutionary dynamics, we
316 selected the proteomes of fifteen species that are highly finished from the 1000
317 Fungal Genomes Project (Table S5). The Hymenochaetales species have median
318 intergenic and intron lengths of 507-634 bp and 59-60 bp, respectively, which are
319 comparable with those observed in genomes of other basidiomycetes. The maximum
320 likelihood phylogeny based on 1,127 single-copy orthologs placed these species with
321 *Fomitiporia mediterranea* and *Schizopora paradoxa*, two other species of the
322 Hymenochaetaceae group with strong bootstrap support (Fig. 1E). This phylogenetic
323 relationship is consistent with previous findings (Larsson et al., 2006), and species
324 with similar genome sizes and pathogenic habits are grouped together. For instance, *P.*
325 *noxius* and *P. lamaensis* with compact genome sizes of ~31 Mb are grouped together,

while the trunk rot pathogens *P. pini* and *F. mediterranea* show an expansion of their genome sizes to 53-63 Mb and are also grouped together.

To explore the genomic architecture underlying the biological attributes of Hymenochaetales, we sought to identify genes and protein domains specific to Hymenochaetales by determining when a new gene family arose and if the family has expanded or contracted. In total, 7,125-11,659 proteins in the Hymenochaetales order are clustered together in 5,184 families. Acquisition of gene families was mainly found at the tips of the phylogeny (531-8,055 families) suggesting each species has a repertoire of specific genes. The seven Hymenochaetaceae species have a total of 62 enriched protein domains compared to other basidiomycetes (Fig. S1). Gain of domains are highlighted such as fungal specific transcription factors (Fungal_trans; 53.8 *vs* 41.6 copies) and peroxidase associated protein domains (Peroxidase_ext; 16.7 *vs* 3.9 copies). These are expected as they are required for efficient degradation of lignin, a tough biopolymer present in woody plants (Dashtban, Schraft, Syed, & Qin, 2010). Consistent with this, CAZymes spanning eight families of lignin-degrading enzymes (AA1-AA8) which include laccases, peroxidases, oxidases, and reductases, and a lytic polysaccharide mono-oxygenase family (LPMO; AA9) were found in all Hymenochaetales species (Table S6).

Genome conservation and specialisation of Phellinus noxius

Although *P. noxius* has a compact genome, 74% (7,313) of its 9,833 predicted genes have orthologs from at least one of the other basidiomycetes, suggesting most of the

349 basidiomycetous core genes are conserved. As a chromosome level assembly is now
350 available in Hymenochaetales, we attempted to characterize chromosome architecture
351 and evolution amongst the Agaricomycotina sub-division. The number of known
352 karyotypes in Basidiomycota ranges from 11 to 14 chromosome pairs (Table S5),
353 which suggests a possible ancestor with similar chromosome numbers. We
354 constructed a linkage network of seven selected species with chromosome sequences
355 based on single-copy orthologs between species pairs. Indeed, we identified 13
356 distinct linkage groups (LG) providing strong evidence that chromosome
357 macro-synteny is largely conserved since the common ancestor of Agaricomycetes
358 (Fig. 2A). Strikingly, such a relationship even extended to Dacrymycetes where
359 multiple scaffolds can be predominantly assigned to different linkage groups, but it is
360 no longer apparent when compared to Tremellomycetes. Certain scaffolds are found
361 to connect different linkage groups, implying inter-chromosomal rearrangements. For
362 example, *P. noxius* scaffold1 is strongly clustered in LG11 but also shows linkage to
363 LG10, implying a translocation from scaffold5 (Fig. 2). Within each linkage group,
364 gene collinearity is no longer apparent, suggesting high levels of intra-chromosomal
365 rearrangements which have been observed in different fungal groups (Hane et al.,
366 2011) (Fig. 2B).
367
368 Consistent with the fact that *P. noxius* is an extremely fast grower (P. Ann et al.,
369 2002), we identified a strikingly 7-fold increase in 1,3-beta-glucan synthase (14
370 compared to an average of 1.8 copies), which is responsible for the formation of
371 beta-glucan components in fungal cell wall (Douglas, 2001). *P. noxius* contains a

372 comprehensive repertoire of carbohydrate-active enzymes; a total of 416 proteins of
373 its proteome were identified as CAZymes (Table S6). This number makes up 4.23%
374 of *P. noxius*'s proteome which is more than those in the other Hymenochaetales,
375 suggesting these genes are necessary and have been retained despite a genome size
376 compaction. Taken together, being able to grow fast and the diversity of the
377 CAZymes encoded in the *P. noxius* genome suggest its capability to infect a wide
378 range of hosts. Additionally, counts of WD40 protein domains are highest in *P.*
379 *noxius* and *P. lamaensis* despite their small genome size (Table S7). This domain is
380 important in protein-protein interactions of cellular networks and is usually associated
381 with additional domains (Leipe, Koonin, & Aravind, 2004). Interrogating this
382 expansion revealed the association of WD40 domains with the AAA and NACHT
383 domains (Table S7), both of which are NTPase domains and such combinations are
384 commonly found in nucleotide-binding-oligomerization-domain like receptors
385 (NLRs). A maximum likelihood phylogeny of the NACHT domain proteins shows
386 different expansions of NLR subfamilies in fungi (Fig. S2). In particular, the
387 C2-NACHT-WD40(n) subfamily has only been found exclusively in a few
388 basidiomycetes (Van der Nest et al., 2014) and is present in the highest copy number
389 in *P. noxius* and *P. lamaensis*. Other expansions include
390 UDP-glucuronosyltransferases, which catalyse conjugation reactions in the
391 biotransformation of xenobiotics released by its host environment (Jancova,
392 Anzenbacher, & Anzenbacherova, 2010).
393
394 *P. noxius displays a bipolar heterothallic mating system*

Determination of mating loci and reproductive mode is considered high-priority in fungal genome analyses as they are the primary determinants of how a fungus expands and generates diversity. Mate recognition of sexual reproduction in Basidiomycota is known to be controlled by two unlinked loci, named as *A* and *B* locus. A conserved head-to-tail orientation of *HD1-HD2* in *HD* pair 1 was found in Hymenochaetales (Fig. 3) which is different from in most species in Agaricomycetes (James et al., 2013). Alignment of 100-kb sequences upstream and downstream of *A* locus in *P. noxius* isolates KPN91, 718-S1 and A42 revealed that *A* locus is highly polymorphic (*HD* pairs in particular) despite well-conserved flanking regions (Fig. S3). For *B* locus, only one *STE3* encoding seven transmembrane helices was identified; four pheromone genes were identified but not physically linked to the highly monomorphic *STE3* (Fig. S4, Table S8, Text S1), which is characteristic of a bipolar mating system.

To further confirm this observation, allele diversity was analyzed by resequencing the *A* and *B* loci from 10 single-basidiospore isolates originating from a single basidiocarp (Table S9). Sequencing of *STE3* revealed two highly similar alleles (b1, b2), with 99.5% amino acid identity. The only variant (244V/A) is considered a semi-conservative mutation (valine and alanine are nonpolar aliphatic acids) and may have minor or no effect on protein function. Previous studies have shown that although STE3 is not involved in mating type determination in bipolar fungi, variations can still be observed (James, Lee, & van Diepen, 2011; James, Srivilai, Kues, & Vilgalys, 2006; Niculita-Hirzel et al., 2008). Primer walking of *A* locus

418 revealed two distinct haplotypes which suggests a heterothallic bipolar reproductive
419 mode in *P. noxius* (Fig. S5): the a1 and a2 alleles of *HD* pair I shared an overall 78%
420 nucleotide identity; the two alleles of *HD* pair II were highly divergent and the HD1
421 domain in a2 allele contains a 1-bp and a 9-bp deletions and has become a
422 pseudogene. The loss of HD1 domain was also found in the *HD* pair I of 718-S1 (Fig.
423 3), suggesting that at least one of the HD1 motifs in *A* locus is dispensable for a
424 functional HD1-HD2 heterodimer in *P. noxius*. The presence or absence of specific
425 HD domains reflects phylogenetic characteristics and has been commonly observed in
426 fungi (Kües, 2015).
427
428 *P. noxius contains a highly polymorphic A locus*
429 Distinct from all the other fungi, *P. noxius* has an exceptionally highly expanded *A*
430 locus across a ~60-kb region (Fig. 3). There are two pairs of HD1-HD2 gene located
431 ~50-kb away from each other. In the case of *P. noxius* KPN91, 14 genes were
432 annotated at the *A locus* (Fig. 3). Orthology analysis placed these genes into 9
433 families that are also present in other fungi (Fig. 4). However, in the genomes of other
434 species, the majority of homologous members of different families are not located in
435 proximity to each other (Fig. 4). This indicates that the large interval in *P. noxius* is a
436 result of accumulating transposition of genes from conserved fungi families not in
437 proximity to *A* locus (Fig. 4). Interestingly, different *P. noxius* isolates display
438 different interval lengths at *A* locus, suggesting that transposition events may be
439 frequent (Fig. 3). Whether transposition plays an additional role in the mating system
440 remains to be clarified.

441

442 *Sequence analysis of 60 P. noxius strains*

443 To further understand the regional dissemination of *P. noxius*, we sequenced the
444 genomes of 60 isolates (Fig 5A) originating from diseased trees across 13 Taiwan and
445 Japanese offshore islands from 2007-2014. This collection was sequenced to a median
446 depth of coverage of 35X. To characterize chromosomal synteny relationship,
447 additional mate pair libraries were sequenced for two isolates (718-S1 and A42). An
448 average of 96% mapping rate was achieved after aligning reads from each strain to
449 the KPN91 reference genome. The descriptions and statistics of the strains are
450 provided in Table S4.

451

452 *Diversification of P. noxius across Pacific Ocean islands*

453 We hypothesized that there may be three populations segregating in this area of
454 Pacific Islands: Taiwan, Ryukyu and Ogasawara islands. To examine the population
455 structure of *P. noxius* in this area, we performed principal-component analysis (Fig.
456 5B) on the SNP variants from individual phased haploid genomes. The major
457 principal component divided Ogasawara islands samples from the rest of the samples,
458 which are located geographically 1,210 km apart. The second and third principal
459 components defined a tight cluster of Taiwanese isolates with considerable overlaps
460 between cities despite being 170 km apart. Most isolates from Ryukyu islands can be
461 differentiated from those from Taiwan (Fig. S6). Interestingly, we identified three
462 isolates from Taiwan that are distinctive from both the Taiwan-Ryukyu and

463 Ogasawara island clusters, suggesting a possibility of more genetically distinct
464 populations within the Taiwan island.
465
466 We constructed a maximum likelihood phylogeny based on 1,837,281 high
467 confidence SNPs of *P. noxius* (Fig. 5C). Concordant with the PCA, the nine isolates
468 from Ogasawara islands form a distinctive lineage, while the 51 Taiwanese and
469 Ryukyu islands isolates are grouped together forming another major lineage. We
470 inferred the population structure in 144,426 unlinked bialleic sites using the Bayesian
471 model-based clustering approach implemented by fastSTRUCTURE (Raj et al., 2014).
472 Consistent with the phylogeny, two Taiwan-Ryukyu and Ogasawara lineages were
473 identified and circulating in this region (highest likelihood with $K = 2$; Fig. 5C).
474 Higher K values shows that the isolates from Ogasawara islands remain one cluster,
475 while the rest of the isolates (independently of their geographical origins) are grouped
476 into genetically homogeneous clusters with little admixture (Fig. S7).
477
478 Further inspection of the phylogeny indicated the possibility of gene flow in this
479 region despite physical separation by the sea. Within the Ogasawara clade, the
480 isolates can be further grouped by their geographical origin (two main islands:
481 Hahajima and Chichijima island separated by 50km) with the exception of KPN334
482 strain. Strain KPN260 was collected from Anijima island which is geographically in
483 proximity to Chichijima island but was grouped with the Hahajima island isolates.
484 Strains collected from within Amami and Okinawa islands are not grouped together
485 on the phylogeny, suggesting independent origins of *P. noxius* infection in both

regions. The pattern of gene flow was more apparent in the 42 isolates collected in two cities of Taiwan, where the isolates were not grouped in the phylogenetic tree according to their geographical origins.

Stable structural variation and intra-isolate polymorphism

The detection of frequency of heterokaryons and polyploids of *P. noxius* in nature remain challenging as its arthospores contain 1-5 nuclei (based on quantification of 145 arthospores from A42 in this study) and multiple allelic fragments in SSRs (2-4 alleles per locus) are commonly found in populations (Akiba et al., 2015; Chung et al., 2015). All the strains were isolated from either a single arthospore or fungal mat, and thus allowed for the analysis of variation in genome structure. We found no deviation in coverage across every scaffold in all strains (Fig. S8), suggesting a stable number of chromosome copies in *P. noxius*. To distinguish the frequency of mono- or heterokaryons in nature, heterozygous SNPs and minor allele frequency (MAF) distribution were inferred in each strain (Fig. 6). We identified four groups (A to D) that clearly differ in heterozygosity and MAF. The group A with the lowest heterozygosity of averaging 0.2 % includes strains 718-S1 and A42, each isolated from a single basidiospore implying they are monokaryotic in nature. All strains in this group exhibited a flat MAF distribution, suggesting that there are spontaneous mutations segregating during the growth of monokaryons that originated at different times. The occurrences of monokaryons are 11% and 47% in the Ogasawara and Taiwan/Ryukyu lineages, respectively. The prevalence of monokaryotic isolates

508 suggests the involvement of basidiospores in disease spread and that heterokaryosis is
509 not required for pathogenicity.
510
511 58% of strains display a much higher heterozygosity, with strain Pn103 having a 1.7%
512 heterozygosity displaying a peak around 50% in MAF distribution. These strains can
513 be further grouped into three categories with distinct MAF profile and
514 heterozygosities (Fig. 6). The largest group of the three (n=19; group D of Fig.6) has
515 on average 1.6% heterozygosity displaying a peak around 50% in MAF distribution,
516 suggesting the presence of two genetically distinct nuclei within the population, i.e.,
517 dikaryons. The remaining two groups did not follow a typical di-karyon MAF
518 distribution, as they peaked around 27%-33% and exhibited different heterozygosities.
519 The deviations may be associated with the number and composition of multiple nuclei
520 in a cell. However, nuclear quantification of seven randomly selected isolates showed
521 no differences between the groups (Fig. S9). These groups may refer to different
522 compositions of two or more genetically distinct nuclei.
523
524 *High nucleotide diversity in P. noxius populations*
525 The *de novo* assemblies of three strains of *P. noxius* have on average 97% nucleotide
526 identity and are largely co-linear to each other with apparent genome translocations
527 between Taiwan/Ryukyu (A42 and KPN91) and the Ogasawara (718-S1) isolate (Fig.
528 S10). We quantified sequence diversity using θs and $\theta \pi$ and categorised them into
529 whole genome average, four-fold synonymous sites and replacement sites (Table 1).
530 A large number of segregating SNPs are found in the genome of *P. noxius*, averaging

one SNP identified in every 20-59 bp. Nucleotide diversity at synonymous sites $\theta\pi$-syn is 15.8 and 19.2 per kilobase in Ogasawara island and Taiwan-Ryukyu populations, respectively. This is ~5 fold higher when compared to the majority of species (Leffler et al., 2012) and is likely an underestimate of true diversity as indels were not considered. Taiwan-Ryukyu lineage has a much higher diversity than Ogasawara which is not due to sample size difference; the same was observed when we reanalyzed with only 9 randomly chosen strains in the Taiwan-Ryukyu populations. Extremely high diversity has been reported in natural populations of *Schizophyllum commune* (Baranova et al., 2015). The Tajima's D is strongly negative in the Taiwan and Ryukyu islands lineage, suggesting an excess of low frequency alleles present in the population possibly as a result of high mutation rate (Baranova et al., 2015) or population expansion. In the Ogasawara population, nucleotide diversity is reduced compared to the Taiwan/Ryukyu lineage and Tajima's D is positive implying a reduced effective population size; *P. noxius* may have been introduced recently in these islands. Together our data suggest that the two *P. noxius* lineages may have derived from genetically distinct gene pools and have undergone divergent evolutionary scenarios, possibly as a result of different time of introduction, different environments, and human interference in Taiwan-Ryukyu *vs* Ogasawara areas.

Candidates for population differentiation

The Taiwan/Ryukyu strains were mainly isolated from diseased trees in urban settings, while the Ogasawara strains were from trails in natural parks (Table S4). Genomic

554 pairwise F_{ST} revealed moderate differentiation (0.12) between the two genetic
555 lineages of *P. noxius*, which is in accordance with both the phylogeny and
556 fastSTRUCTURE analyses. We identified genomic regions that may contain potential
557 candidates for such environmental origins by investigating 99.9% tail for observed
558 F_{ST} 5-kb windows (Fig. 7). This definition revealed 13 outlier regions. Gene ontology
559 analyses of 42 genes within these regions did not reveal any GO enrichment terms,
560 indicating the sites showing evidence of differentiation may be involved in different
561 functions. Interestingly, the largest region spanning 12 kb at scaffold 6 contains four
562 genes. Homologs from three of the genes are implicated in fungal cell wall
563 organization and fruiting body formation (PNOK_0653900; (Szeto, Leung, & Kwan,
564 2007)), salt tolerance (PNOK_0654000; (Steffens, Brautigam, Jakoby, & Hulskamp,
565 2015)), and plant cell wall degradation (PNOK_0654100; xylanase). These are all
566 possible drivers for population differentiation (Apse, Aharon, Snedden, & Blumwald,
567 1999).
568

569 ## Discussion

570 Here we report four high-quality genome sequences of Hymenochaetales species that
571 are global tree pathogens of particular importance. To date chromosome-level
572 assemblies are available only for a few basidiomycetous species (Manuel Alfaro et al.,
573 2016; Foulongne-Oriol et al., 2016; J. E. Stajich et al., 2010) including *P. noxius*
574 (Table S5). Orthologous relationships with other complete genomes of
575 basidiomycetes have confirmed conservation of karyotypes with few fusion or breaks

576 in Agaricomycetes. Our study has shown the diversity and abundance of CAZymes,
577 in particularly lignin-degrading enzymes, in the genomes of Hymenochaetaceae
578 species. Such genetic architecture has been demonstrated in other white rot fungi
579 (Riley et al., 2014), and differences in CAZymes have been implicated as the genetic
580 basis of softwood or hardwood utilization (Suzuki et al., 2012). As revealed by
581 comparative genomics analysis, *P. noxius* has highly expanded 1,3-beta-glucan
582 synthase genes and abundant CAZymes, making it an aggressive wood decay
583 pathogen of a wide variety of both broadleaved and coniferous trees. The results can
584 serve as a starting point for understanding the ecological role of *P. noxius*. Our study
585 also identified high copy numbers of C2-NACHT-WD40(n)-containing NLRs and
586 candidate genes associated with population differentiation. The NLR family is highly
587 diverse in fungi and was found to be central to the process of programmed cell death
588 and implicated in fungal vegetative incompatibility and general nonself recognition
589 (Bidard, Clave, & Saupe, 2013). Analysis of global transcription at different
590 pathogenesis stages and detailed functional assays will help resolve their functions.
591
592 Population genomics analyses of *P. noxius* suggest that it is a hypervariable species.
593 Our investigations into mating type loci and genome-wide heterozygosity further
594 indicated that the genetic hyperdiversity can be attributed to a bipolar heterothallic
595 reproductive system and heterokaryotic nature, though gene flow and/or high
596 mutation rate may also play some role. The characteristic large interval between *HD*
597 pairs has only been reported in *Schizophyllum commune* (~55 kb) and *Flammulina*
598 *velutipes* (~70 kb), in which the genomic separation likely emerged through

599 inversions or transpositions of gene clusters surrounding *HD* (van Peer et al., 2011).
600 This exceptional large separation between *HD* pairs would allow higher probability of
601 recombination between the physically distant *HD* genes(James et al., 2013; van Peer
602 et al., 2011), thus resulting in progeny with more diverse mating types which are
603 ready to mate. Notably, both monokaryotic and heterokaryotic state of *P. noxius*
604 mycelia are prevalent in the nature, and some isolates likely contain more than two
605 genetically different nuclei (Chung et al., 2015). In addition, some isolates were able
606 to produce basidiocarps by themselves when cultured on sawdust medium (P.-J. Ann,
607 pers. comm.), suggesting dikaryotization or homokaryotic fruiting occurred
608 spontaneously or in response to certain conditions (Wendland, 2016). It would be
609 interesting to further investigate the complex regulatory mechanisms underlying
610 anastomosis, karyogamy, and meiotic division during vegetative growth and
611 basidiocarp formation. Transcriptional diversity among genetically variable
612 individuals is also warrant further exploration.
613
614 How *P. noxius* is spread in regions of Asia has been the focus of a few studies (Akiba
615 et al., 2015; Chung et al., 2015; Hattori, Abe, & Usugi, 1996). Genomic analysis of
616 the strains from across Taiwan and offshore islands of Japan allowed us to re-examine
617 possible mode of disease transmission in the Asia Pacific region. The pattern of gene
618 flow within and between islands suggested that human activity such as planting of
619 infected seedlings may have promoted the movement of *P. noxius*. which provides an
620 artificial environment for population to increase. The within-population
621 hyperdiversity, prevalence of monokaryotic isolates, and sporadic pattern of new

622 disease foci also support the involvement of basidiospores in *P. noxius* dissemination.
623 Considering its host range and fast-growing ability in warm weather, and the
624 abundant basidiospores that can be produced from perennial fruiting bodies with huge
625 dispersal potential (e.g., the basidiospores of *Heterobasidion annosum* and
626 *Peniophora aurantiaca* were captured 50–500 km and ~1000 km apart from the
627 inoculum source), *P. noxius* may potentially affect more agricultural, ecological, and
628 residential environments. A preliminary model based on 19 bioclimatic variables of
629 known locations of ~100 *P. noxius* isolates from south eastern Asia, Australia, and
630 Pacific islands predicted that extensive global regions are at risk, which includes a big
631 part of the South American continent (Klopfenstein et al., 2016).
632
633 The Hymenochaetales is phylogenetically placed between the better-studied
634 Agaricales and Ustillaginales orders, making the reference assembly of *P. noxius*
635 KPN91 an attractive genome to study the evolutionary transition between these orders
636 of Basidiomycota. It should be of continuous interest to confirm this observation
637 when more reference genome assemblies become available. Genetic hyperdiversity of
638 *P. noxius* suggests that the pathogen may have greater adaptability to different
639 environments and stresses. Associating growth phenotypes under a variety of
640 conditions to the variations identified in this study will be a logical next step for a full
641 understanding of the genetic basis underlying the fitness and virulence of white root
642 rot fungi. For disease control and prevention, much more attention needs to be paid to
643 monitor how these fungi will behave in changing or extreme weather conditions.
644

Figures and Tables

Fig 1. Life stages of *P. noxius* and comparative genomic analysis of Hymenochaetales species. (**a**) The mycelial mat with young creamy leading front and aged brown section. (**b**) In advanced stage of decay, the hyphae form a network of brown zone lines permeating the soft and white wood tissue. (Lower left and lower right) (**c and d**) Basidiocarps are perennial and can be resupinate (**c**) or grow into a sessile bracket-like conk with a broad basal attachment (**d**). The distinctive greyish-brown surface is the hymenial layer with irregularly polygonal pores, containing four-spored basidia, ellipsoid and hyaline basidiospores, but no hymenial setae. (**e**) The phylogeny of four *Phellinus* species with 15 other species of Basidiomycota based on a concatenated alignment of single-copy orthologous genes. All nodes have 100 out of 100 bootstrap replicates. The numbers of gained ("+") and lost ("-") gene families along each branch of the phylogeny is annotated.

Fig 2. Linkage group (LG) network of Basidiomycota. (**a)** The linkage groups were identified by linking single-copy orthologs of scaffolds between species pairs. All scaffolds included in this plot are larger than 500 kb. Each directional edge points toward the reference chromosome. Edges were weighted by the number of single-copy orthologs, and an edge was filtered if it has a weight smaller than 20 or less than 40% of the sum of all weights out of a node. (**b)** Cross-mapping of single-copy orthologs in LG10 and 11. Scaffold names are shown at the upper-right side of each sequence, with detectable telomeric regions labelled as 'T' at the upper-left side.

Fig 3. Synteny around the *A* mating locus. The analysis included *Phellinus noxius*, *Porodaedalea pini*, *Phellinus sulphurascens*, *Phellinus lamaensis*, two other species

674 from Hymenochaetales species (*Fomitiporia mediterranea, Schizopora paradoxa*),
675 two species from Agaricales (*Laccaria bicolar, Coprinopsis cinerea*),
676 *Sistotremastrum niveocremeum,* and *Ustilago maydis*.
677
678 **Fig 4. Orthology network of genes in the *A* locus of *P. noxius.*** Each node in this
679 plot represents a gene. An edge is added if two genes are in proximity (physically
680 separated by less than two genes). Numbers next to the edges and nodes are number
681 of occurrences of different combinations of genes in each species. For example, 77
682 members of OG0000015 orthogroup in *P. lamaensis* are found adjacent to each other
683 on the genome. Another 37 members of this orthogroup are dispersed throughout the
684 genome and are not located in proximity to any members of the 9 orthogroups.
685
686 **Fig 5. The population genomics of 60 *P. noxius* isolates.** (**a**) Map of Taiwan and
687 offshore islands of Japan showing origins of the 60 sampled *P. noxius* isolates.
688 Ogasawara islands were conveniently drawn below Ryukyu islands so this does not
689 represent their actual location. (**b**) PCA plot of 60 *P. noxius* isolates using
690 genome-wide variation data sampled from 13 islands by the first three eigenvectors.
691 (**c**) Top: Phylogenetic tree with 100 bootstrap using SNPs computed from alignment
692 to KPN91 reference. Point separating the Taiwan-Ryukyu and Ogasawara island
693 isolates was used as root. Nodes with >90% bootstrap were labelled with circles.
694 Bottom: fastSTRUCTURE analysis of the linkage independent pruned set of variation
695 data. A model with two ancestral components (K=2) had the highest likelihood to
696 explain the variation of genome-wide structure on the 60 isolates. Also see Fig. S7 for
697 different K.
698
699 **Fig 6. Heterozygosity and allele frequencies of *P. noxius.*** (a) Boxplot showing
700 abundances of heterozygous SNPs inferred in each *P. noxius* isolate can be
701 categorised into four groups. (b) Density plot of minor allele frequencies (MAF) of
702 heterozygous SNPs in 60 isolates of *P. noxius*. *Asterisk denote group containing two
703 isolates that were cultured from basidiospores.

Fig. 7 Weighted F_{ST} values for 5kb windows across the *P. noxius* assembly. Red colour dots indicate windows having F_{ST} value greater than 99.9% tail of 0.55. The 12-kb candidate region is marked in blue star. Annotations and references of genes located in this candidate region are listed.

Table 1. Polymorphism in the two regional lineages of *P. noxius*.

716 **Availability of data and materials:**

717 Genome assemblies and annotations are available from NCBI under whole genome
718 shotgun (WGS) ID: NBII00000000 (*P. noxius*), NBBA00000000 (*P. sulphurascens*),
719 NBAY00000000 (*P. pini*) and NBAZ00000000 (*P. lamaensis*). Bioproject and
720 Biosample ID of raw data are available in Table S1 and S2.

721

722 **Author's contributions:**

723 Strain cultivation and preparation: H.H.L., T.J.L, H.M.K, M.A., T.H., Y.O., N.S. and
724 T.K. Strain provider: C.L.C., R.F.L., S.S.T., P.J.A., J.N.T., M.A., T.H., Y.O., N.S.
725 Strain sequencing and assembly: C.L.C., H.H.L., C.Y.C., M.J.L., T.K. and I.J.T.
726 Annotation and manual curation: H.M.K., T.J.L and I.J.T. Comparative genomics
727 analysis: T.H.K, D.L., M.B.R., H.M.K. and I.J.T. Population genomics analysis:
728 H.M.K., T.J.L and I.J.T. Mating locus analysis: C.L.C., H.H.L., Y.Y.C., T.H.K., I.J.T.
729 RNA-seq analysis: T.J.L and I.J.T. Wrote the manuscript: C.L.C, T.J.L, H.H.L, T.K
730 and I.J.T. Conceived and directed the project: C.L.C., T.K. and I.J.T.

731

732 **Acknowledgements**

733 We thank John Wang (Biodiversity Research Center, Academia Sinica), Yen-Ping
734 Hsueh (IMB, Academia Sinica) and Robert Waterhouse (University of Lausanne) for
735 commenting the manuscript. We thank Chian-mei Wei, Kuan-chun Chen (High
736 Throughput Genomics Core at Biodiversity Research Center, Academia Sinica) for
737 sequencing. We thank Tun-Tschu Chang and Yu-Ching Huang for strain collection
738 and consultation.

739

740 **Funding:**

741 I.J.T. and J.T.L were funded by Ministry of Science and Technology
742 (105-2628-B-001-002-MY3 and 105-2313-B-001 -003). C.L.C., H.H.L. and Y.Y.C
743 were funded by the Office of General Affairs, National Taiwan University.

744

References

Akiba, M., Ota, Y., Tsai, I. J., Hattori, T., Sahashi, N., & Kikuchi, T. (2015). Genetic Differentiation and Spatial Structure of Phellinus noxius, the Causal Agent of Brown Root Rot of Woody Plants in Japan. *Plos One*, *10*(10), e0141792. doi:10.1371/journal.pone.0141792

Alexa, A., & Rahnenfuhrer, J. (2016). topGO: Enrichment Analysis for Gene Ontology. *R package version 2.26.0*.

Alfaro, M., Castanera, R., Lavin, J. L., Grigoriev, I. V., Oguiza, J. A., Ramirez, L., & Pisabarro, A. G. (2016). Comparative and transcriptional analysis of the predicted secretome in the lignocellulose-degrading basidiomycete fungus Pleurotus ostreatus. *Environ Microbiol*, *18*(12), 4710-4726. doi:10.1111/1462-2920.13360

Ann, P., Chang, T., & Ko, W. (2002). Phellinus noxius Brown Root Rot of Fruit and Ornamental Trees in Taiwan. *Plant Disease*, *86*.

Ann, P. J., Lee, H. L., & Huang , T. C. (1999). Brown Root Rot of 10 Species of Fruit Trees Caused by Phellinus noxius in Taiwan. *Plant Disease*, *83*(8), 746-750.

Apse, M. P., Aharon, G. S., Snedden, W. A., & Blumwald, E. (1999). Salt tolerance conferred by overexpression of a vacuolar Na+/H+ antiport in Arabidopsis. *Science*, *285*(5431), 1256-1258.

Bankevich, A., Nurk, S., Antipov, D., Gurevich, A. A., Dvorkin, M., Kulikov, A. S., . . . Pevzner, P. A. (2012). SPAdes: A New Genome Assembly Algorithm and Its Applications to Single-Cell Sequencing. *Journal of Computational Biology*, *19*(5), 455-477. doi:10.1089/cmb.2012.0021

Baranova, M. A., Logacheva, M. D., Penin, A. A., Seplyarskiy, V. B., Safonova, Y. Y., Naumenko, S. A., . . . Kondrashov, A. S. (2015). Extraordinary Genetic Diversity in a Wood Decay Mushroom. *Mol Biol Evol*, *32*(10), 2775-2783. doi:10.1093/molbev/msv153

Bidard, F., Clave, C., & Saupe, S. J. (2013). The transcriptional response to nonself in the fungus Podospora anserina. *G3 (Bethesda)*, *3*(6), 1015-1030. doi:10.1534/g3.113.006262

Bolger, A. M., Lohse, M., & Usadel, B. (2014). Trimmomatic: a flexible trimmer for Illumina sequence data. *Bioinformatics*, *30*(15), 2114-2120. doi:10.1093/bioinformatics/btu170

778 Borodovsky, M., & Lomsadze, A. (2011). Eukaryotic gene prediction using
779 GeneMark.hmm-E and GeneMark-ES. *Curr Protoc Bioinformatics, Chapter 4*,
780 Unit 4 6 1-10. doi:10.1002/0471250953.bi0406s35
781 Butler, J., MacCallum, I., Kleber, M., Shlyakhter, I. A., Belmonte, M. K., Lander, E.
782 S., . . . Jaffe, D. B. (2008). ALLPATHS: de novo assembly of whole-genome
783 shotgun microreads. *Genome Res, 18*(5), 810-820. doi:10.1101/gr.7337908
784 Castanera, R., Lopez-Varas, L., Borgognone, A., LaButti, K., Lapidus, A., Schmutz,
785 J., . . . Ramirez, L. (2016). Transposable Elements versus the Fungal Genome:
786 Impact on Whole-Genome Architecture and Transcriptional Profiles. *PLoS*
787 *Genet*, *12*(6), e1006108. doi:10.1371/journal.pgen.1006108
788 Chain, P. S., Grafham, D. V., Fulton, R. S., Fitzgerald, M. G., Hostetler, J., Muzny,
789 D., . . . Detter, J. C. (2009). Genomics. Genome project standards in a new era
790 of sequencing. *Science*, *326*(5950), 236-237. doi:10.1126/science.1180614
791 Chang, C. C., Chow, C. C., Tellier, L. C., Vattikuti, S., Purcell, S. M., & Lee, J. J.
792 (2015). Second-generation PLINK: rising to the challenge of larger and richer
793 datasets. *Gigascience, 4*, 7. doi:10.1186/s13742-015-0047-8
794 Chang, T.-T. (1992). Decline of some forest trees associated with brown root rot
795 caused by Phellinus noxius. *Plant Pathology Bulletin, 1*(2), 90-95.
796 Chin, C.-S., Alexander, D. H., Marks, P., Klammer, A. A., Drake, J., Heiner, C., . . .
797 Korlach, J. (2013). Nonhybrid, finished microbial genome assemblies from
798 long-read SMRT sequencing data. *Nature Methods, 10*(6), 563-569.
799 doi:10.1038/nmeth.2474
800 Chin, C.-S., Peluso, P., Sedlazeck, F. J., Nattestad, M., Concepcion, G. T., Clum,
801 A., . . . Schatz, M. C. (2016). Phased diploid genome assembly with
802 single-molecule real-time sequencing. *Nature Methods, 13*(12), 1050-1054.
803 doi:10.1038/nmeth.4035
804 Chung, C.-L., Huang, S.-Y., Huang, Y.-C., Tzean, S.-S., Ann, P.-J., Tsai, J.-N., . . .
805 Liou, R.-F. (2015). The Genetic Structure of Phellinus noxius and
806 Dissemination Pattern of Brown Root Rot Disease in Taiwan. *Plos One*,
807 *10*(10), e0139445. doi:10.1371/journal.pone.0139445
808 Conesa, A., Gotz, S., Garcia-Gomez, J. M., Terol, J., Talon, M., & Robles, M. (2005).
809 Blast2GO: a universal tool for annotation, visualization and analysis in
810 functional genomics research. *Bioinformatics, 21*(18), 3674-3676.
811 doi:10.1093/bioinformatics/bti610

812 Cunniffe, N. J., Cobb, R. C., Meentemeyer, R. K., Rizzo, D. M., & Gilligan, C. A.
813 (2016). Modeling when, where, and how to manage a forest epidemic,
814 motivated by sudden oak death in California. *Proc Natl Acad Sci U S A,*
815 *113*(20), 5640-5645. doi:10.1073/pnas.1602153113
816 Danecek, P., Auton, A., Abecasis, G., Albers, C. A., Banks, E., DePristo, M. A., . . .
817 Genomes Project Analysis, G. (2011). The variant call format and VCFtools.
818 *Bioinformatics, 27*(15), 2156-2158. doi:10.1093/bioinformatics/btr330
819 Dashtban, M., Schraft, H., Syed, T. A., & Qin, W. (2010). Fungal biodegradation and
820 enzymatic modification of lignin. *Int J Biochem Mol Biol, 1*(1), 36-50.
821 Douglas, C. M. (2001). Fungal beta(1,3)-D-glucan synthesis. *Med Mycol, 39 Suppl 1*,
822 55-66.
823 Emms, D. M., & Kelly, S. (2015). OrthoFinder: solving fundamental biases in whole
824 genome comparisons dramatically improves orthogroup inference accuracy.
825 *Genome Biol, 16*, 157. doi:10.1186/s13059-015-0721-2
826 Felsenstein, J. (2005). PHYLIP (Phylogeny Inference Package) version 3.6.
827 *Distributed by the author. Department of Genome Sciences, University of*
828 *Washington, Seattle*.
829 Finn, R. D., Coggill, P., Eberhardt, R. Y., Eddy, S. R., Mistry, J., Mitchell, A. L., . . .
830 Bateman, A. (2016). The Pfam protein families database: towards a more
831 sustainable future. *Nucleic Acids Research, 44*(D1), D279-D285.
832 doi:10.1093/nar/gkv1344
833 Fisher, M. C., Henk, D. A., Briggs, C. J., Brownstein, J. S., Madoff, L. C., McCraw, S.
834 L., & Gurr, S. J. (2012). Emerging fungal threats to animal, plant and
835 ecosystem health. *Nature, 484*(7393), 186-194. doi:10.1038/nature10947
836 Floudas, D., Binder, M., Riley, R., Barry, K., Blanchette, R. A., Henrissat, B., . . .
837 Hibbett, D. S. (2012). The Paleozoic origin of enzymatic lignin decomposition
838 reconstructed from 31 fungal genomes. *Science, 336*(6089), 1715-1719.
839 doi:10.1126/science.1221748
840 Foulongne-Oriol, M., Rocha de Brito, M., Cabannes, D., Clément, A., Spataro, C.,
841 Moinard, M., . . . Savoie, J.-M. (2016). The Genetic Linkage Map of the
842 Medicinal Mushroom Agaricus subrufescens Reveals Highly Conserved
843 Macrosynteny with the Congeneric Species Agaricus bisporus. *G3:*
844 *Genes|Genomes|Genetics, 6*(5), 1217-1226. doi:10.1534/g3.115.025718
845 Garrison, E., & Marth, G. (2012). Haplotype-based variant detection from short-read
846 sequencing. *arXiv, 1207*, 3907.

847 Goberville, E., Hautekeete, N. C., Kirby, R. R., Piquot, Y., Luczak, C., & Beaugrand,
848 G. (2016). Climate change and the ash dieback crisis. *Sci Rep, 6*, 35303.
849 doi:10.1038/srep35303
850 Grigoriev, I. V., Nikitin, R., Haridas, S., Kuo, A., Ohm, R., Otillar, R., . . . Shabalov, I.
851 (2014). MycoCosm portal: gearing up for 1000 fungal genomes. *Nucleic Acids*
852 *Research, 42*(D1), D699-D704. doi:10.1093/nar/gkt1183
853 Gross, A., Holdenrieder, O., Pautasso, M., Queloz, V., & Sieber, T. N. (2014).
854 Hymenoscyphus pseudoalbidus, the causal agent of European ash dieback.
855 *Mol Plant Pathol, 15*(1), 5-21. doi:10.1111/mpp.12073
856 Guy, L., Roat Kultima, J., & Andersson, S. G. E. (2010). genoPlotR: comparative
857 gene and genome visualization in R. *Bioinformatics, 26*(18), 2334-2335.
858 doi:10.1093/bioinformatics/btq413
859 Hane, J. K., Rouxel, T., Howlett, B. J., Kema, G. H., Goodwin, S. B., & Oliver, R. P.
860 (2011). A novel mode of chromosomal evolution peculiar to filamentous
861 Ascomycete fungi. *Genome Biol, 12*(5), R45. doi:10.1186/gb-2011-12-5-r45
862 Hattori, T., Abe, Y., & Usugi, T. (1996). Distribution of clones of *Phellinus noxius* in
863 a windbreak on Ishigaki Island. *European Journal of Forest Pathology, 26*(2),
864 69-80. doi:10.1111/j.1439-0329.1996.tb00711.x
865 Hepting, G. H. (1971). *Diseases of forest and shade trees of the United States*: U.S.
866 Dept. Of Agriculture Forest Service Handbook Number 386.
867 Hoff, K. J., Lange, S., Lomsadze, A., Borodovsky, M., & Stanke, M. (2016).
868 BRAKER1: Unsupervised RNA-Seq-Based Genome Annotation with
869 GeneMark-ET and AUGUSTUS. *Bioinformatics, 32*(5), 767-769.
870 doi:10.1093/bioinformatics/btv661
871 Huang, H., Sun, L., Bi, K., Zhong, G., & Hu, M. (2016). The effect of
872 phenazine-1-carboxylic acid on the morphological, physiological, and
873 molecular characteristics of *Phellinus noxius*. *Molecules, 21*(5), 613.
874 Hunt, M., Kikuchi, T., Sanders, M., Newbold, C., Berriman, M., & Otto, T. D. (2013).
875 REAPR: a universal tool for genome assembly evaluation. *Genome biology,*
876 *14*, R47. doi:10.1186/gb-2013-14-5-r47
877 James, T. Y., Lee, M., & van Diepen, L. T. (2011). A single mating-type locus
878 composed of homeodomain genes promotes nuclear migration and
879 heterokaryosis in the white-rot fungus Phanerochaete chrysosporium.
880 *Eukaryot Cell, 10*(2), 249-261. doi:10.1128/EC.00212-10

James, T. Y., Srivilai, P., Kues, U., & Vilgalys, R. (2006). Evolution of the bipolar mating system of the mushroom Coprinellus disseminatus from its tetrapolar ancestors involves loss of mating-type-specific pheromone receptor function. *Genetics, 172*(3), 1877-1891. doi:10.1534/genetics.105.051128

James, T. Y., Sun, S., Li, W., Heitman, J., Kuo, H. C., Lee, Y. H., . . . Olson, A. (2013). Polyporales genomes reveal the genetic architecture underlying tetrapolar and bipolar mating systems. *Mycologia, 105*(6), 1374-1390. doi:10.3852/13-162

Jancova, P., Anzenbacher, P., & Anzenbacherova, E. (2010). Phase II drug metabolizing enzymes. *Biomed Pap Med Fac Univ Palacky Olomouc Czech Repub, 154*(2), 103-116.

Jones, P., Binns, D., Chang, H.-Y., Fraser, M., Li, W., McAnulla, C., . . . Hunter, S. (2014). InterProScan 5: genome-scale protein function classification. *Bioinformatics, 30*(9), 1236-1240. doi:10.1093/bioinformatics/btu031

Kamper, J., Kahmann, R., Bolker, M., Ma, L. J., Brefort, T., Saville, B. J., . . . Birren, B. W. (2006). Insights from the genome of the biotrophic fungal plant pathogen Ustilago maydis. *Nature, 444*(7115), 97-101. doi:10.1038/nature05248

Katoh, K., & Standley, D. M. (2014). MAFFT: iterative refinement and additional methods. *Methods Mol Biol, 1079*, 131-146. doi:10.1007/978-1-62703-646-7_8

Klopfenstein, N. B., Pitman, E. W. I., Hanna, J. W., Cannon, P. G., Stewart, J. E., Sahashi, N., . . . Kim, M.-S. (2016). *A preliminary bioclimatic approach to predicting potential distribution of Phellinus noxious and geographical areas at risk from invasion.* Paper presented at the Proceedings of the 63rd Annual Western International Forest Disease Work Conference.

Koboldt, D. C., Zhang, Q., Larson, D. E., Shen, D., McLellan, M. D., Lin, L., . . . Wilson, R. K. (2012). VarScan 2: Somatic mutation and copy number alteration discovery in cancer by exome sequencing. *Genome research, 22*(3), 568-576. doi:10.1101/gr.129684.111

Kües, U. (2015). From two to many: multiple mating types in Basidiomycetes. *Fungal Biology Reviews, 29*(3–4), 126-166. doi:http://dx.doi.org/10.1016/j.fbr.2015.11.001

914 Kumar, S., Stecher, G., & Tamura, K. (2016). MEGA7: Molecular Evolutionary
915 Genetics Analysis Version 7.0 for Bigger Datasets. *Mol Biol Evol*, *33*(7),
916 1870-1874. doi:10.1093/molbev/msw054
917 Kurtz, S., Phillippy, A., Delcher, A. L., Smoot, M., Shumway, M., Antonescu, C., &
918 Salzberg, S. L. (2004). Versatile and open software for comparing large
919 genomes. *Genome Biology*, *5*(2), R12.
920 Lam, K. K., LaButti, K., Khalak, A., & Tse, D. (2015). FinisherSC: a repeat-aware
921 tool for upgrading de novo assembly using long reads. *Bioinformatics*, *31*(19),
922 3207-3209. doi:10.1093/bioinformatics/btv280
923 Larsson, K.-H., Parmasto, E., Fischer, M., Langer, E., Nakasone, K. K., & Redhead, S.
924 a. (2006). Hymenochaetales: a molecular phylogeny for the hymenochaetoid
925 clade. *Mycologia*, *98*, 926-936.
926 Lavezzo, E., Falda, M., Fontana, P., Bianco, L., & Toppo, S. (2016). Enhancing
927 protein function prediction with taxonomic constraints--The Argot2.5 web
928 server. *Methods*, *93*, 15-23. doi:10.1016/j.ymeth.2015.08.021
929 Leffler, E. M., Bullaughey, K., Matute, D. R., Meyer, W. K., Segurel, L., Venkat,
930 A., . . . Przeworski, M. (2012). Revisiting an old riddle: what determines
931 genetic diversity levels within species? *PLoS Biol*, *10*(9), e1001388.
932 doi:10.1371/journal.pbio.1001388
933 Leipe, D. D., Koonin, E. V., & Aravind, L. (2004). STAND, a class of P-loop
934 NTPases including animal and plant regulators of programmed cell death:
935 multiple, complex domain architectures, unusual phyletic patterns, and
936 evolution by horizontal gene transfer. *J Mol Biol*, *343*(1), 1-28.
937 doi:10.1016/j.jmb.2004.08.023
938 Li, H., Handsaker, B., Wysoker, A., Fennell, T., Ruan, J., Homer, N., . . . Durbin, R.
939 (2009). The Sequence Alignment/Map format and SAMtools. *Bioinformatics*
940 *(Oxford, England)*, *25*, 2078-2079. doi:10.1093/bioinformatics/btp352
941 Loftus, B. J., Fung, E., Roncaglia, P., Rowley, D., Amedeo, P., Bruno, D., . . . Hyman,
942 R. W. (2005). The genome of the basidiomycetous yeast and human pathogen
943 Cryptococcus neoformans. *Science*, *307*(5713), 1321-1324.
944 doi:10.1126/science.1103773
945 Martin, F., Aerts, A., Ahren, D., Brun, A., Danchin, E. G., Duchaussoy, F., . . .
946 Grigoriev, I. V. (2008). The genome of Laccaria bicolor provides insights into
947 mycorrhizal symbiosis. *Nature*, *452*(7183), 88-92. doi:10.1038/nature06556

948 Maurer-Stroh, S., & Eisenhaber, F. (2005). Refinement and prediction of protein
949 prenylation motifs. *Genome biology, 6*(6), R55.
950 Min, B., Park, H., Jang, Y., Kim, J. J., Kim, K. H., Pangilinan, J., . . . Choi, I. G.
951 (2015). Genome sequence of a white rot fungus Schizopora paradoxa
952 KUC8140 for wood decay and mycoremediation. *J Biotechnol, 211*, 42-43.
953 doi:10.1016/j.jbiotec.2015.06.426
954 Morin, E., Kohler, A., Baker, A. R., Foulongne-Oriol, M., Lombard, V., Nagy, L.
955 G., . . . Martin, F. (2012). Genome sequence of the button mushroom Agaricus
956 bisporus reveals mechanisms governing adaptation to a humic-rich ecological
957 niche. *Proc Natl Acad Sci U S A, 109*(43), 17501-17506.
958 doi:10.1073/pnas.1206847109
959 Nagy, L. G., Riley, R., Tritt, A., Adam, C., Daum, C., Floudas, D., . . . Hibbett, D. S.
960 (2016). Comparative Genomics of Early-Diverging Mushroom-Forming Fungi
961 Provides Insights into the Origins of Lignocellulose Decay Capabilities. *Mol*
962 *Biol Evol, 33*(4), 959-970. doi:10.1093/molbev/msv337
963 Nandris, D., Nicole, M., & Geiger, J. P. (1987). Variation in virulence among
964 Rigidoporus lignosus and Phellinus noxius isolates from West Africa1.
965 *European Journal of Forest Pathology, 17*(4-5), 271-281.
966 doi:10.1111/j.1439-0329.1987.tb01026.x
967 Niculita-Hirzel, H., Labbe, J., Kohler, A., le Tacon, F., Martin, F., Sanders, I. R., &
968 Kues, U. (2008). Gene organization of the mating type regions in the
969 ectomycorrhizal fungus Laccaria bicolor reveals distinct evolution between
970 the two mating type loci. *New Phytol, 180*(2), 329-342.
971 doi:10.1111/j.1469-8137.2008.02525.x
972 Ohm, R. A., de Jong, J. F., Lugones, L. G., Aerts, A., Kothe, E., Stajich, J. E., . . .
973 Wosten, H. A. (2010). Genome sequence of the model mushroom
974 Schizophyllum commune. *Nat Biotechnol, 28*(9), 957-963.
975 doi:10.1038/nbt.1643
976 Olson, A., Aerts, A., Asiegbu, F., Belbahri, L., Bouzid, O., Broberg, A., . . . Stenlid, J.
977 (2012). Insight into trade-off between wood decay and parasitism from the
978 genome of a fungal forest pathogen. *New Phytol, 194*(4), 1001-1013.
979 doi:10.1111/j.1469-8137.2012.04128.x
980 Parra, G., Bradnam, K., & Korf, I. (2007). CEGMA: a pipeline to accurately annotate
981 core genes in eukaryotic genomes. *Bioinformatics (Oxford, England), 23*,
982 1061-1067. doi:10.1093/bioinformatics/btm071

983 Potter, C., Harwood, T., Knight, J., & Tomlinson, I. (2011). Learning from history,
984 predicting the future: the UK Dutch elm disease outbreak in relation to
985 contemporary tree disease threats. *Philos Trans R Soc Lond B Biol Sci, 366*(1573), 1966-1974. doi:10.1098/rstb.2010.0395
987 Price, M. N., Dehal, P. S., & Arkin, A. P. (2009). FastTree: Computing Large
988 Minimum Evolution Trees with Profiles instead of a Distance Matrix.
989 *Molecular Biology and Evolution, 26*(7), 1641-1650.
990 doi:10.1093/molbev/msp077
991 Raj, A., Stephens, M., & Pritchard, J. K. (2014). fastSTRUCTURE: Variational
992 Inference of Population Structure in Large SNP Data Sets. *Genetics, 197*(2),
993 573-589. doi:10.1534/genetics.114.164350
994 Riley, R., Salamov, a. a., Brown, D. W., Nagy, L. G., Floudas, D., Held, B. W., . . .
995 Grigoriev, I. V. (2014b). Extensive sampling of basidiomycete genomes
996 demonstrates inadequacy of the white-rot/brown-rot paradigm for wood decay
997 fungi. *Proceedings of the National Academy of Sciences*.
998 doi:10.1073/pnas.1400592111
999 Sahashi, N., Akiba, M., Ishihara, M., Miyazaki, K., & Kanzaki, N. (2010). Cross
1000 Inoculation Tests with Phellinus noxius Isolates from Nine Different Host
1001 Plants in the Ryukyu Islands, Southwestern Japan. *Plant Disease, 94*(3),
1002 358--360.
1003 Sahashi, N., Akiba, M., Ishihara, M., Ota, Y., & Kanzaki, N. (2012). Brown root rot
1004 of trees caused by Phellinus noxius in the Ryukyu Islands, subtropical areas of
1005 Japan. *Forest Pathology, 42*, 353-361.
1006 Sahashi, N., Akiba, M., Takemoto, S., Yokoi, T., Ota, Y., & Kanzaki, N. (2014).
1007 Phellinus noxius causes brown root rot on four important conifer species in
1008 Japan. *European Journal of Plant Pathology, 140*(4), 869--873.
1009 Schwartz, S., Zhang, Z., Frazer, K. A., Smit, A., Riemer, C., Bouck, J., . . . Miller, W.
1010 (2000). PipMaker--a web server for aligning two genomic DNA sequences.
1011 *Genome Research, 10*(4), 577--586.
1012 Schwarze, F., Jauss, F., Spencer, C., Hallam, C., & Schubert, M. (2012). Evaluation
1013 of an antagonistic Trichoderma strain for reducing the rate of wood
1014 decomposition by the white rot fungus Phellinus noxius. *Biological Control, 61*(2), 160--168.
1016 Simão, F. A., Waterhouse, R. M., Ioannidis, P., Kriventseva, E. V., & Zdobnov, E. M.
1017 (2015). BUSCO: assessing genome assembly and annotation completeness

with single-copy orthologs. *Bioinformatics, 31*(19), 3210-3212. doi:10.1093/bioinformatics/btv351

Stajich, J. E., Wilke, S. K., Ahren, D., Au, C. H., Birren, B. W., Borodovsky, M., . . . Pukkila, P. J. (2010). Insights into evolution of multicellular fungi from the assembled chromosomes of the mushroom Coprinopsis cinerea (Coprinus cinereus). *Proceedings of the National Academy of Sciences, 107*(26), 11889-11894. doi:10.1073/pnas.1003391107

Stamatakis, A. (2006). RAxML-VI-HPC: maximum likelihood-based phylogenetic analyses with thousands of taxa and mixed models. *Bioinformatics (Oxford, England), 22*, 2688-2690. doi:10.1093/bioinformatics/btl446

Stanke, M., Tzvetkova, A., & Morgenstern, B. (2006). AUGUSTUS at EGASP: using EST, protein and genomic alignments for improved gene prediction in the human genome. *Genome biology, 7 Suppl 1*, S11.11-18. doi:10.1186/gb-2006-7-s1-s11

Steffens, A., Brautigam, A., Jakoby, M., & Hulskamp, M. (2015). The BEACH Domain Protein SPIRRIG Is Essential for Arabidopsis Salt Stress Tolerance and Functions as a Regulator of Transcript Stabilization and Localization. *PLoS Biol, 13*(7), e1002188. doi:10.1371/journal.pbio.1002188

Suzuki, H., MacDonald, J., Syed, K., Salamov, A., Hori, C., Aerts, A., . . . Master, E. R. (2012). Comparative genomics of the white-rot fungi, Phanerochaete carnosa and P. chrysosporium, to elucidate the genetic basis of the distinct wood types they colonize. *BMC Genomics, 13*(1). doi:10.1186/1471-2164-13-444

Szeto, C. Y., Leung, G. S., & Kwan, H. S. (2007). Le.MAPK and its interacting partner, Le.DRMIP, in fruiting body development in Lentinula edodes. *Gene, 393*(1-2), 87-93. doi:10.1016/j.gene.2007.01.030

Van der Nest, M. A., Olson, A., Lind, M., Velez, H., Dalman, K., Brandstrom Durling, M., . . . Stenlid, J. (2014). Distribution and evolution of het gene homologs in the basidiomycota. *Fungal Genet Biol, 64*, 45-57. doi:10.1016/j.fgb.2013.12.007

van Peer, A. F., Park, S.-Y., Shin, P.-G., Jang, K.-Y., Yoo, Y.-B., Park, Y.-J., . . . Kong, W.-S. (2011). Comparative genomics of the mating-type loci of the mushroom *Flammulina velutipes* reveals widespread synteny and recent inversions. *Plos One, 6*(7), e22249. doi:10.1371/journal.pone.0022249

1052 Vilella, A. J., Blanco-Garcia, A., Hutter, S., & Rozas, J. (2005). VariScan: Analysis
1053 of evolutionary patterns from large-scale DNA sequence polymorphism data.
1054 *Bioinformatics, 21*(11), 2791-2793. doi:10.1093/bioinformatics/bti403
1055 Walker, B. J., Abeel, T., Shea, T., Priest, M., Abouelliel, A., Sakthikumar, S., . . . Earl,
1056 A. M. (2014). Pilon: An Integrated Tool for Comprehensive Microbial Variant
1057 Detection and Genome Assembly Improvement. *Plos One, 9*(11), e112963.
1058 doi:10.1371/journal.pone.0112963
1059 Weber, T., Blin, K., Duddela, S., Krug, D., Kim, H. U., Bruccoleri, R., . . . Medema,
1060 M. H. (2015). antiSMASH 3.0—a comprehensive resource for the genome
1061 mining of biosynthetic gene clusters. *Nucleic Acids Research, 43*(W1),
1062 W237-W243. doi:10.1093/nar/gkv437
1063 Wences, A. H., & Schatz, M. C. (2015). Metassembler: merging and optimizing de
1064 novo genome assemblies. *Genome biology, 16*(1).
1065 doi:10.1186/s13059-015-0764-4
1066 Wendland, J. (2016). *Growth, Differentiation and Sexuality* (J. Wendland Ed. 3 ed.):
1067 Springer.
1068 Williams, H. L., Sturrock, R. N., Islam, M. A., Hammett, C., Ekramoddoullah, A. K.,
1069 & Leal, I. (2014). Gene expression profiling of candidate virulence factors in
1070 the laminated root rot pathogen Phellinus sulphurascens. *BMC Genomics, 15*,
1071 603. doi:10.1186/1471-2164-15-603
1072 Wu, J., Peng, S. L., Zhao, H. B., Tang, M. H., Li, F. R., & Chen, B. M. (2011).
1073 Selection of species resistant to the wood rot fungus *Phellinus noxius*.
1074 *European Journal of Plant Pathology, 130*(4), 463-467.
1075 doi:10.1007/s10658-011-9774-6
1076 Yin, Y., Mao, X., Yang, J., Chen, X., Mao, F., & Xu, Y. (2012). dbCAN: a web
1077 resource for automated carbohydrate-active enzyme annotation. *Nucleic Acids*
1078 *Res, 40*(Web Server issue), W445-451. doi:10.1093/nar/gks479
1079 Zhou, L.-W., Vlasák, J., & Dai, Y.-C. (2016). Taxonomy and phylogeny of
1080 *Phellinidium* (Hymenochaetales, Basidiomycota): A redefinition and the
1081 segregation of *Coniferiporia* gen. nov. for forest pathogens. *Fungal Biology*,
1082 *120*(8), 988-1001. doi:http://dx.doi.org/10.1016/j.funbio.2016.04.008
1083 Zuccaro, A., Lahrmann, U., Guldener, U., Langen, G., Pfiffi, S., Biedenkopf, D., . . .
1084 Kogel, K. H. (2011). Endophytic life strategies decoded by genome and
1085 transcriptome analyses of the mutualistic root symbiont Piriformospora indica.
1086 *PLoS Pathog, 7*(10), e1002290. doi:10.1371/journal.ppat.1002290

1087

1088

1089

1090


a


b


c


d

e

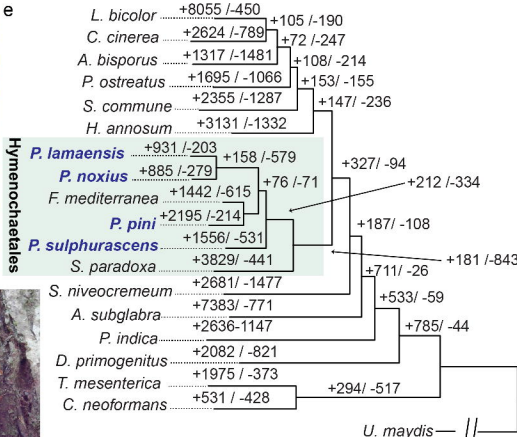
L. bicolor
+8055 /-450
+105 /-190
C. cinerea
+2624 /-789
+72 /-247
A. bisporus
+1317 /-1481
+108/ -214
P. ostreatus
+1695 / -1066
+153/ -155
S. commune
+2355 /-1287
+147/ -236
H. annosum
+3131 /-1332
Hymenochaetales
P. lamaensis
+931 /-203
+158 /-579
P. noxius
+885 /-279
+76 /-71
F. mediterranea
+1442 /-615
P. pini
+2195 /-214
P. sulphurascens
+1556/ -531
S. paradoxa
+3829/ -441
+327/ -94
+212 /-334
+187/ -108
+181 /-843
+711/ -26
S. niveocremeum
+2681/ -1477
A. subglabra
+7383/ -771
+533/ -59
P. indica
+2636-1147
+785/ -44
D. primogenitus
+2082 / -821
T. mesenterica
+1975 / -373
C. neoformans
+531 / -428
+294/ -517
U. maydis
0.3

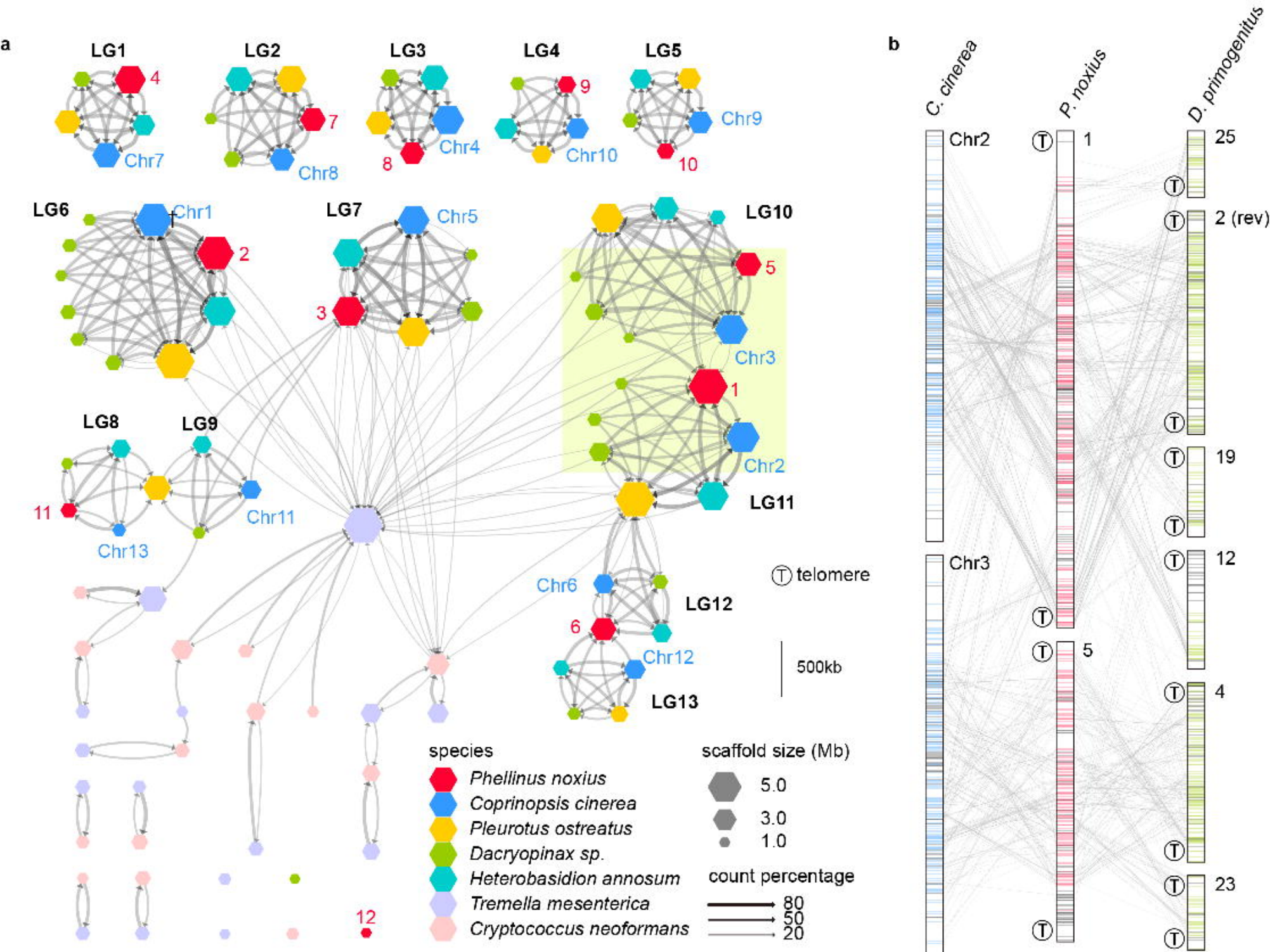
a
LG1
LG2
LG3
LG4
LG5
LG6
LG7
LG8
LG9
LG10
LG11
LG12
LG13
Chr1
Chr2
Chr3
Chr4
Chr5
Chr6
Chr7
Chr8
Chr9
Chr10
Chr11
Chr12
Chr13
telomere
500kb
species
Phellinus noxius
Coprinopsis cinerea
Pleurotus ostreatus
Dacryopinax sp.
Heterobasidion annosum
Tremella mesenterica
Cryptococcus neoformans
scaffold size (Mb)
5.0
3.0
1.0
count percentage
80
50
20
b
C. cinerea
P. noxius
D. primogenitus
Chr2
Chr3
1
5
25
2 (rev)
19
12
4
23

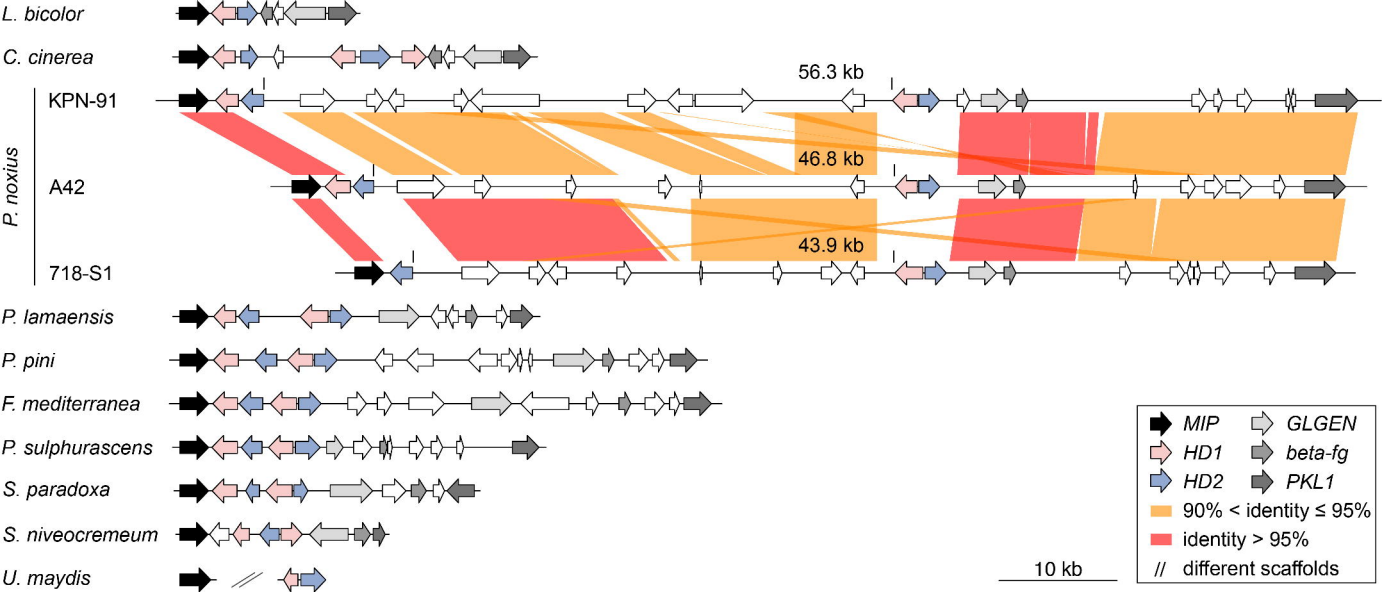
L. bicolor
C. cinerea
P. noxius
KPN-91
A42
718-S1
56.3 kb
46.8 kb
43.9 kb
P. lamaensis
P. pini
F. mediterranea
P. sulphurascens
S. paradoxa
S. niveocremeum
U. maydis
MIP
HD1
HD2
GLGEN
beta-fg
PKL1
90% < identity ≤ 95%
identity > 95%
// different scaffolds
10 kb

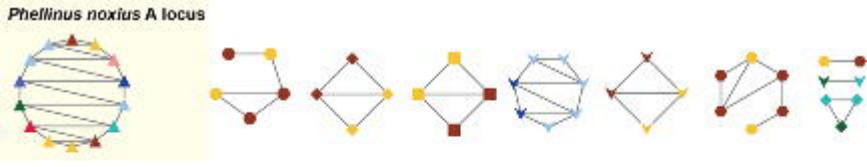
Phellinus noxius A locus
37 28 41 17 1 1 42
3 3 3 2 1 1 1
4 2 2 2 2 4
1 11 77
2 35 1
12 27
Orthogroup
OG0000015
OG0000069
OG0000212
OG0000759
OG0001120
OG0001374
OG0005630
OG0007218
OG0042637
Species
Porodaedalea pini
Phellinus sulphurascens
Schizophyllum commune
Coprinopsis cinerea
Phellinus lamaensis
Phellinus noxius

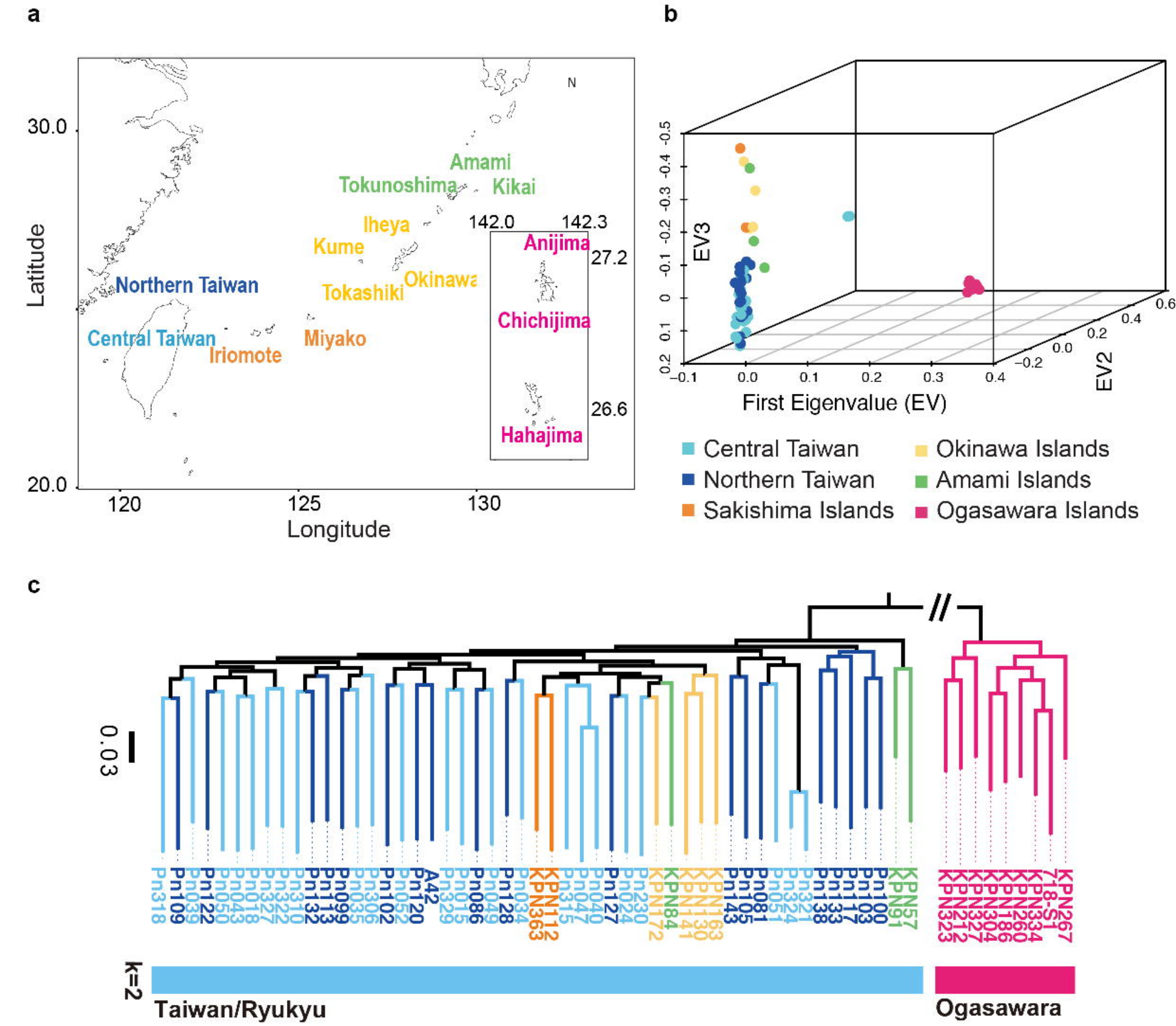
a
b
c
Latitude
Longitude
30.0
20.0
120
125
130
142.0
142.3
27.2
26.6
N
Amami
Tokunoshima
Kikai
Iheya
Kume
Anijima
Okinawa
Tokashiki
Northern Taiwan
Chichijima
Central Taiwan
Miyako
Iriomote
Hahajima
EV3
EV2
First Eigenvalue (EV)
Central Taiwan
Northern Taiwan
Sakishima Islands
Okinawa Islands
Amami Islands
Ogasawara Islands
0.03
k=2
Taiwan/Ryukyu
Ogasawara

a

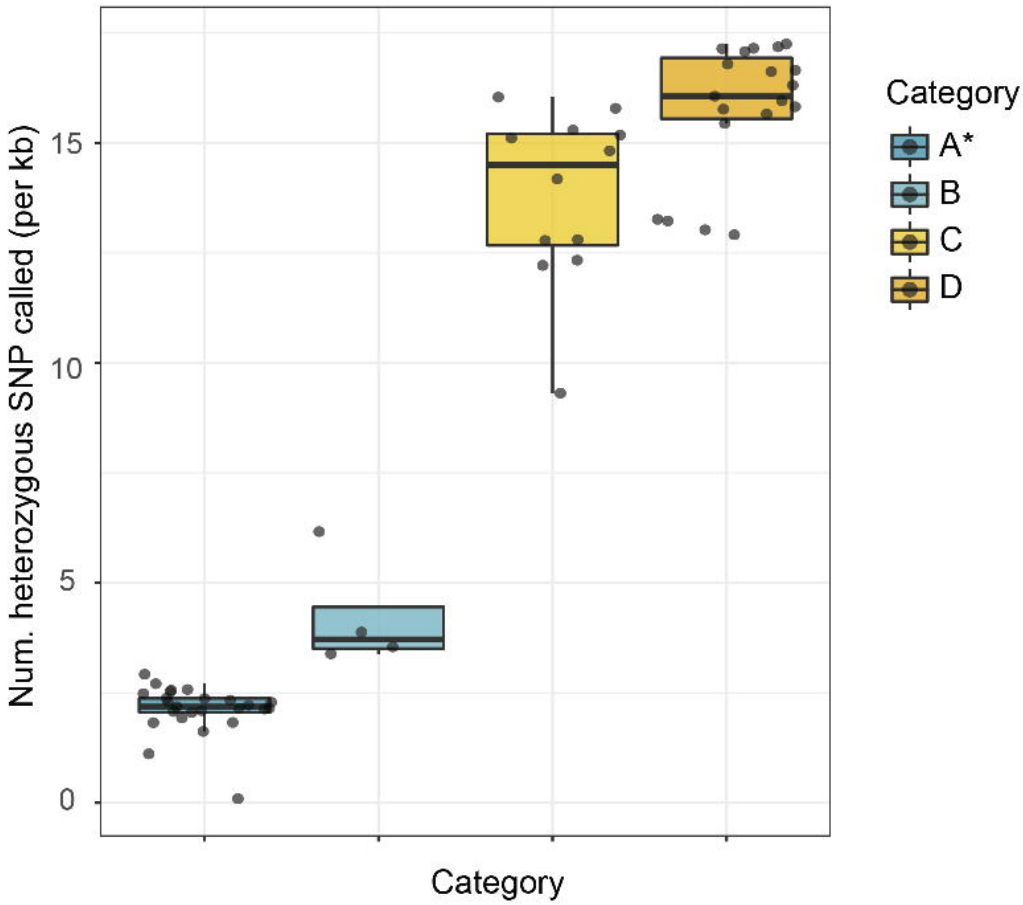
Num. heterozygous SNP called (per kb)
0
5
10
15
Category
Category
A*
B
C
D

b

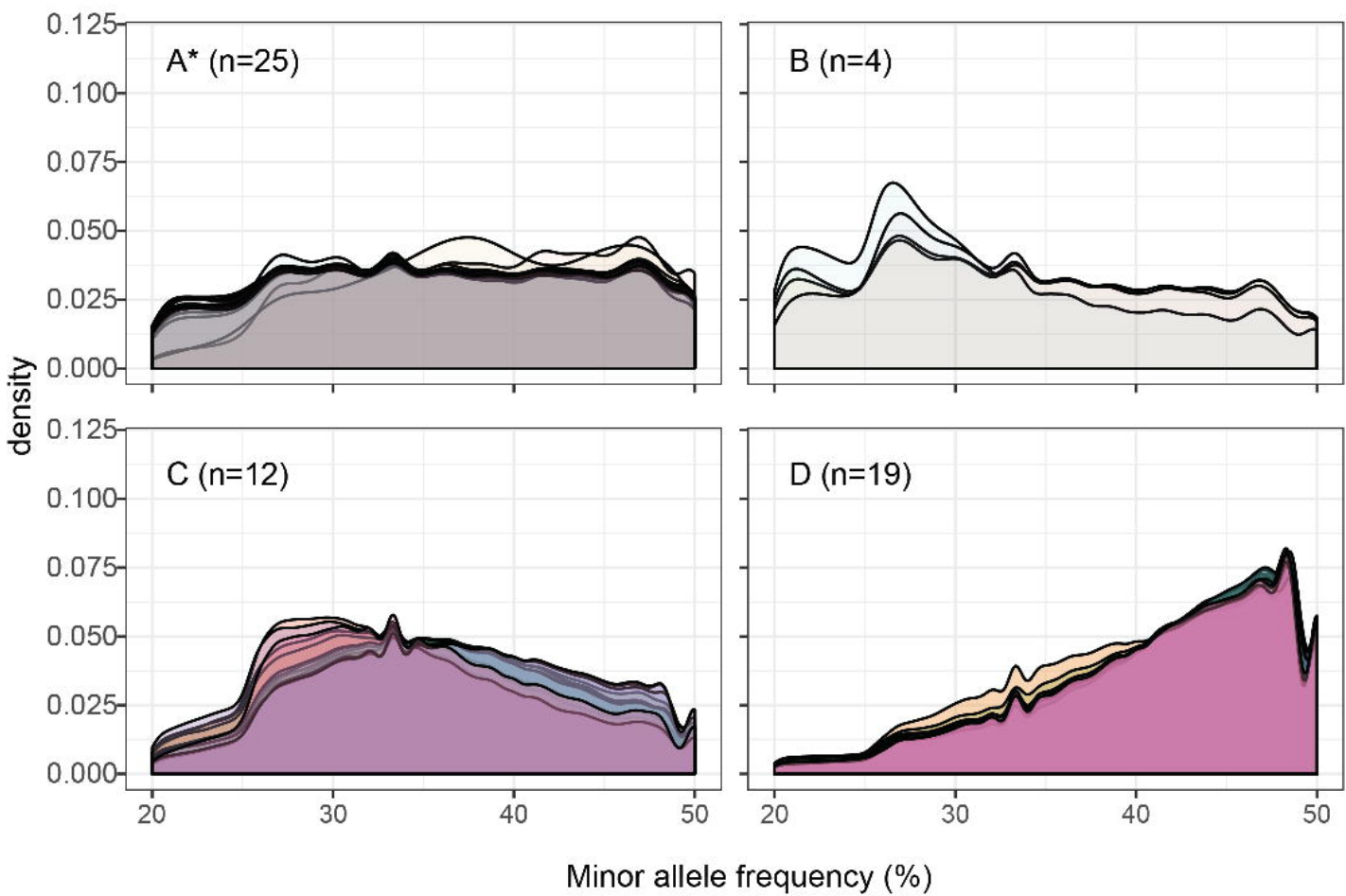
A* (n=25)
B (n=4)
C (n=12)
D (n=19)
density
0.125
0.100
0.075
0.050
0.025
0.000
20
30
40
50
Minor allele frequency (%)

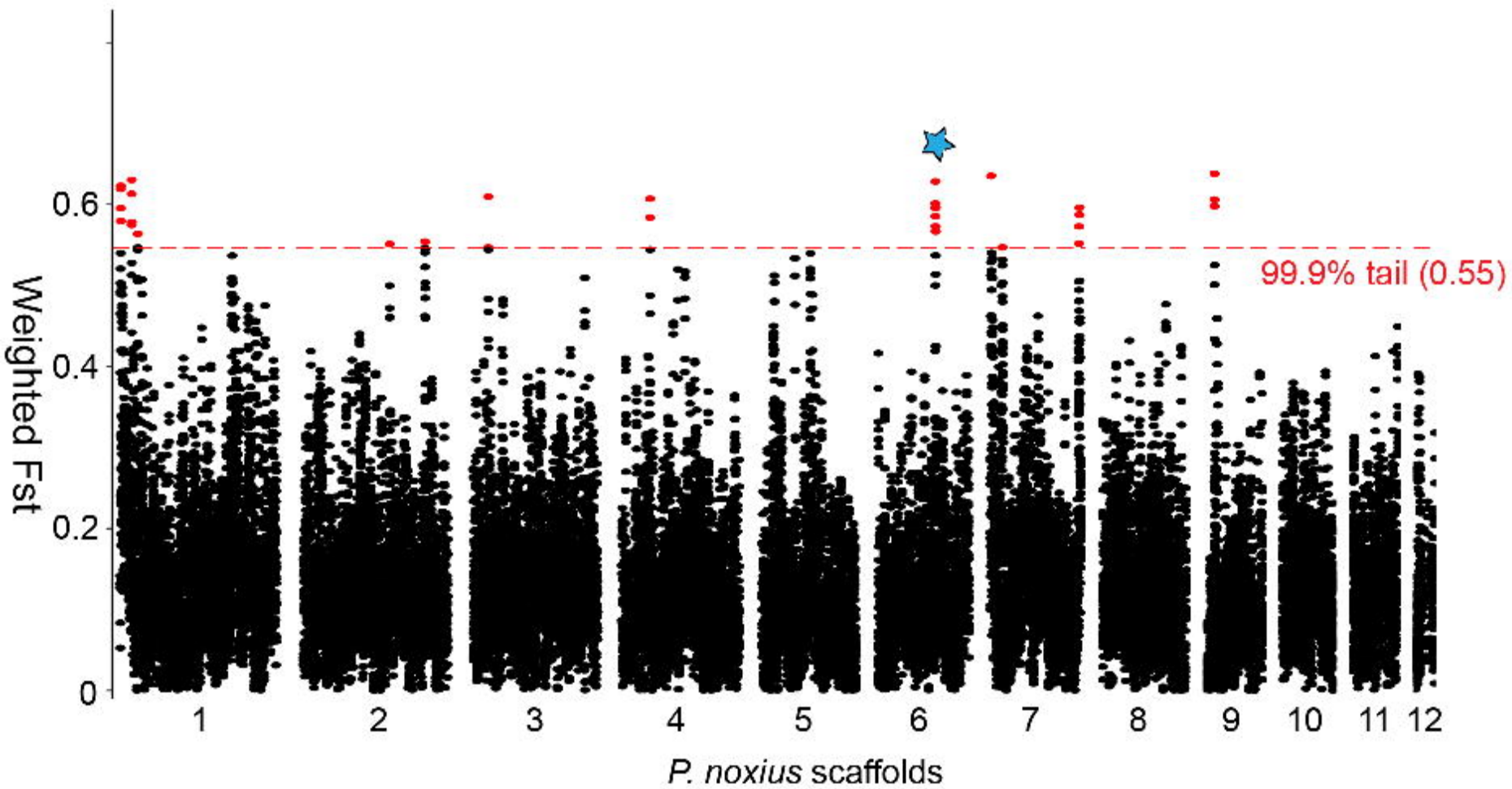

Gene ID	Product Description	Reference of homologs
PNOK_0653900	glycosylphosphatidylinositol-anchored	Szeto *et al.*, 2007
PNOK_0654000	BEACH-domain-containing protein	Steffens *et al.*, 2015
PNOK_0654100	endo-1,4-beta xylanase	Bray and Clark (1994)
PNOK_0654200	hypothetical protein	N/A

Population	Analyzed Sites	Segregating sites (S)	Singletons	θπ (x1,000)	θs (x1,000)	Tajima's D
Whole genome						
Ogasawara (n=9)	30,028,158	506,231	174,924	6.6	6.3	0.3
TaiwanRyukyu (n=51)	31,376,691	1,538,598	545,324	8.0	10.9	-0.9
TaiwanRyukyu subset (n=9)[1]	30,640,276	749,681	408,021	8.1	8.9	-0.5
Synonymous Sites						
Ogasawara (n=9)	4,651,751	182,879	59,464	15.8	14.7	0.4
TaiwanRyukyu (n=51)	4,758,211	513,717	161,353	19.2	23.6	-0.7
TaiwanRyukyu subset (n=9)[1]	4,704,161	269,060	136,780	19.3	20.5	-0.4
Replacement Sites						
Ogasawara (n=9)	9,794,069	71,497	25,981	2.9	2.8	0.2
TaiwanRyukyu (n=51)	10,018,114	230,689	93,385	3.6	5.3	-1.2
TaiwanRyukyu subset (n=9)[1]	9,904,211	103,907	60,313	3.6	4.0	-0.6

[1] A random of nine isolates were chosen to repeat the analysis.